Waveform Design and Optimization for Integrated Visible Light Positioning and Communication

Shuai Ma, *Member, IEEE*, Shiyu Cao, Hang Li, Songtao Lu, *Member, IEEE*, Tingting Yang, Youlong Wu, *Member, IEEE*, Naofal Al-Dhahir, *Fellow, IEEE*, and Shiyin Li

Abstract— In this paper, we investigate an energy efficient waveform design for integrated visible light positioning and communication (VLPC) systems by exploiting the relationship between visible light positioning (VLP) and visible light communication (VLC). We propose that the direct current component and the alternating current component of the VLPC signals are utilized for positioning and communication, respectively. With a single LED-lamp, we propose a received-signal-strength based 3D VLP scheme, and further derive the Cramer-Rao lower bound (CRLB). Then, by exploiting the inherent coupling relationship between VLP and VLC, the positioning results are utilized for channel estimation of VLC, which can significantly reduce the channel estimation pilot overhead. Furthermore, we optimize the waveform design by minimizing the CRLB, while satisfying both the outage probability of communication rate and total transmit power constraints. However, this problem turns to be non-convex and intractable. To address this challenging problem, we utilize the Conditional Value-at-Risk to conservatively transform the outage probability constraint into a deterministic form. By exploiting the block coordinate descent algorithm, the waveform design problem can be efficiently solved by alternately optimizing VLP and VLC convex sub-problems and dual problem. Finally, simulation results verify both the effectiveness and robustness of the proposed waveform design.

Index Terms— Visible light communication, visible light positioning, waveform design, beamforming optimization.

I. INTRODUCTION

WITH the tremendous growth of massive connectivity and bandwidth-hungry applications of Internet of things (IoT) networks, the spectrum crisis of the fifth generation (5G) has become more and more serious [1]. Since people spend about 87% of their time in indoor activities [2], it is inevitable that the indoor network connectivities and positioning services become more crucial. By utilizing light emitting diodes (LEDs), visible light communication (VLC) and visible light positioning (VLP), with an abundant unregulated bandwidth in the 400-790 THz band, can provide high-speed-data transmission and high accuracy positioning in indoor environments, which are two promising technologies for the future indoor IoT networks [3], [4], [5], [6], such as homes, offices, airports, supermarkets, hospitals and factories.

On the one hand, by exploiting the off-the-shelf photodiode (PD) as a receiver, VLC has several distinct advantages, including low power consumption, high data rate, massive connectivity, high secrecy, and no interference on radio frequency (RF) networks [7]. A number of prior studies have considered the optimization of VLC systems [8], [9], [10] to guarantee different quality-of service (QoS) requirements for IoT applications. Specifically, the optimal power allocation schemes of non-orthogonal multiple access (NOMA) VLC networks were proposed in [8] for both static and mobile users. For direct-current-biased optical orthogonal frequency division multiplexing (DCO-OFDM) VLC, both the direct current (DC)-offset and subcarriers power are jointly optimized in [9] to enhance the information transmission rate. In [10], the authors present an improved run-length limited (RLL) codes to decrease bit error rate (BER) and mitigate LED flicker with a high throughput. At the same time, VLC industry standards are continuously evolving, where standardization efforts for specific VLC applications have taken place in the scope of the Information Technology Industries Association (JEITA) [11] and IEEE Standards Association (IEEE-SA) [12], [13].

On the other hand, VLP has recently drawn great attention, due to the directionality of light signals and low multi-path

effects, which provides high positioning accuracy for indoor IoT devices. The VLP technique estimates the PDs' locations by extracting features of the received visible light signals and uses the lamp as the anchor node. So far, various algorithms have been studied in VLP system, and the key measurements include received signal strength (RSS) [14], [15], [16], time of arrival (TOA) [17], [18], time difference of arrival (TDOA) [19], and angle of arrival (AOA) [20]. Compared to TOA and TDOA, the complexity of RSS is low and does not require synchronization [21].

For practical indoor IoT applications, both communication and positioning functions are required simultaneously. However, integrated visible light positioning and communication (VLPC) is still in its infancy, and only few works have investigated integrated VLPC systems. For example, a VLC system is demonstrated to achieve positioning based on orthogonal frequency division multiplexing access (OFDMA) [22], [23]. A VLPC system is designed in [24] by using filter bank multicarrier-based subcarrier multiplexing (FBMC-SCM). Based on an OFDMA VLPC network, the authors in [25] propose to control the access point (AP) selection, bandwidth allocation, adaptive modulation, and power allocation to maximize the data rate while guaranteeing positioning accuracy constraints. In [26], a modified experience replay actor-critic (MERAC) reinforcement learning approach is proposed to maximize the sum rate while guaranteeing the users' minimum data rates and positioning accuracy constraints. In [27], the authors introduce a coordinated resource allocation approach for the system to maximize the sum rate under minimum data rates and positioning accuracy constraints for the devices.

In the existing VLPC works [22], [23], [24], communication and positioning are implemented in different frequency bands, i.e., OFDM and Filter Bank Multi-Carrier (FBMC), which will increase the bandwidth requirement and lead to low spectral efficiency. Besides, the existing VLPC works [22], [23], [24] apply the multi-lamp based setup to realize the positioning functionality, which may not be applicable in many practical VLC applications. For example, in a long corridor, the lamps usually are installed in a line, the PDs can only receive the signals from one lamp due to the limited field of view (FOV), and thus applications of the multi-lamp based positioning schemes are limited. Moreover, some fundamental questions about VLPC have not been well addressed, including: What is the coupling relationship between positioning and communication in VLPC systems? What is the optimal trade-off between positioning and communication? How to design an integrated waveform to achieve positioning and communication at the same time?

To overcome the issues of both low spectral efficiency and limited application scenarios faced by the existing VLPC schemes, we propose an integrated VLPC scheme based on a single LED-lamp in this paper, where both communication and positioning are implemented in the same frequency band. Furthermore, to address the above fundamental issues of VLPC, we propose a novel waveform design framework for VLPC systems, and exploit the inherent coupling relationship between positioning and communication to optimize the

waveform design. The main contributions of this papers are summarized as follows:

- Unlike the traditional VLC system that often filters out the DC component, in which the positioning and communication signals are differentiated and transmitted through different frequency bands, we propose a novel integrated VLPC waveform design framework to exploit the DC component of the signal for positioning, and the alternating current (AC) component for communications, which can significantly improve energy efficiency. To the best of our knowledge, this class of waveform design is proposed for integrated VLPC systems for the first time.

- By considering a VLPC system that includes a mobile user equipment (UE) with multiple PD and a single LED lamp as a base station (BS), we formulate a 3D positioning problem as a non-linear least squares (NLS) optimization, where the orientation of the mobile UE can be arbitrary. By leveraging the Armijo-Wolfe step-size calculation rule, we propose a modified Newton method to iteratively solve the 3D positioning NLS problem. Furthermore, to theoretically evaluate the positioning performance, we derive the Cramer-Rao lower bound (CRLB) expression to quantify the performance of the VLPC system.

- We reveal the inherent coupling relationship between positioning and communication in the integrated VLPC system. Specifically, by exploiting the fact that the channel state information (CSI) of the line-of-sight (LOS) link is a deterministic function of the PDs' position and orientation, the positioning results of VLP can be utilized for CSI estimation in VLC, which can significantly reduce the overhead of transmitting channel estimation pilot sequences. Then, with the On-Off Keying (OOK) based waveform design, we derive both an exact achievable rate expression and its closed-form lower bound.

- Furthermore, we investigate the optimal waveform design for the integrated VLPC system. Specifically, by jointly optimizing the AC component, DC component and the receiver beamformer, we aim to minimize the positioning errors, i.e., the CRLB of VLP, while satisfying the outage probability constraint of the VLC rate, and total power constraint. To overcome the difficulty brought by the probabilistic constraint, we adopt the conservative approximation method of Conditional Value-at-Risk (CVaR), which transforms the chance constraints into a more tractable deterministic form. Then, by adopting the block coordinate descent (BCD) algorithm, the optimal waveform design optimization problem can be efficiently solved by alternately optimizing VLP and VLC convex sub-problems.

The rest of this paper is organized as follows. The VLPC system model and the integrated VLPC waveform design framework are presented in Section II. In Section III, the RSS-based 3D positioning scheme is proposed and the CRLB is derived. In Section IV, we analyze the relationship between positioning and communication, and derive the achievable rate of the VLPC system. In Section V, we optimize the integrated

TABLE I
SUMMARY OF MAIN ACRONYMS AND KEY NOTATIONS

Notation	Description
VLPC	Visible light positioning and communication
DC	Direct current
AC	Alternating current
UE	User equipment
RSS	Received signal strength
FIM	Fisher information matrix
CRLB	Cramer-Rao lower bound
CSI	Channel state information
CVaR	Conditional Value-at-Risk
BCD	Block coordinate descent
s	Information signal with zero mean and unit power
I_{DC}	DC component
P	AC power
$\mathbf{u}_{\mathrm{L}}$	The position of the LED
$\mathbf{u}_i$	The position of the ith PD
$\mathbf{n}_i$	The orientation of the ith PD
$\mathbf{e}$	Positioning error
$\Delta\mathbf{h}$	Estimated CSI error
$\mathbf{I}_{\mathrm{F}}$	FIM of Positioning
$\mathbf{w}$	Receiving beamformer

VLPC waveform design. In Section VI, the corresponding simulation results are presented and analyzed. Finally, Section VII concludes this paper. In addition, Table I summarizes the main acronyms and key notations in this paper.

Notations: Boldfaced lowercase and uppercase letters represent vectors and matrices, respectively. $\mathbb{S}^n$ represents the space of n-dimensional real symmetric matrices while $\mathbb{R}^n$ represents the space of n-dimensional real matrices. The rank and trace of a matrix are denoted as $\mathrm{rank}\,(\cdot)$ and $\mathrm{Tr}\,(\cdot)$, repectively. $\mathbb{E}\,[\cdot]$ stands for the expectation, s.t. is short for subject to, $\|\cdot\|$ specifies the Euclidean norm, $[\cdot]^{\mathrm{T}}$ represents the transposition of vector or matrix, $\mathrm{Pr}\,\{\cdot\}$ is the probability and $\mathcal{K} \triangleq \{1, 2, \cdots, K\}$.

II. INTEGRATED VLPC SYSTEM MODEL

Consider an integrated VLPC system, as shown in Fig. 1, where a single LED lamp serving as the BS serves a mobile UE with K PDs and an inertial measurement unit (IMU). Assume that the PDs are placed rigidly on the UE, i.e., all PDs rotate along with the UE, and both the orientation and the rotation angle of the UE can be calculated based on the IMU. The transmitted signal of the LED includes a DC component (DC-bias) I_{DC} and an AC component $\sqrt{P}s$, where s denotes the information signal with zero mean and unit power, i.e., $\mathbb{E}\,[s] = 0$ and $\mathbb{E}\,[s^2] = 1$, and $P > 0$ denotes the power gain of the power amplifier. Moreover, the DC component I_{DC} is used for positioning, and the AC component $\sqrt{P}s$ is used for data transmission. The detailed descriptions of I_{DC} and $\sqrt{P}s$ are given later.
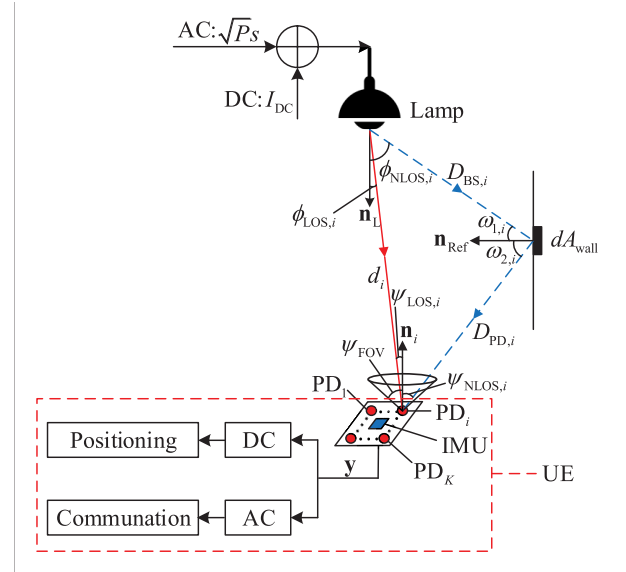

Fig. 1. The integrated VLPC system model.

The mobile UE receives the signal through the LOS and the reflection channels. Let $\mathbf{y} \triangleq \{y_i\}_{i=1}^K = [y_1, \ldots, y_K]^{\mathrm{T}}$ represent the UE received signal, where y_i denotes the received signal of the ith PD, and $i \in \mathcal{K}$. Then, the received signal $\mathbf{y}$ will be decomposed into the DC component and the AC component.

Let $\mathbf{u}_{\mathrm{L}} = [\vartheta_1, \vartheta_2, \vartheta_3]^{\mathrm{T}}$ and $\mathbf{u}_i = [\theta_{1,i}, \theta_{2,i}, \theta_{3,i}]^{\mathrm{T}}$ denote the positions of the LED lamp and the ith PD, respectively, where $i \in \mathcal{K}$. Moreover, assume that the orientation of the LED lamp is vertical downward, which is denoted by $\mathbf{n}_{\mathrm{L}} = [0, 0, -1]^{\mathrm{T}}$. Due to the fixed relative position of PDs, without loss of generality, let the position of the 1st PD represent the position of the UE and assume that the orientation and the rotation angle of the 1st PD are the same as that of UE. For the ith PD, let $\mathbf{n}_{0,i} \in \mathbb{R}^{3 \times 1}$ denote the initial orientation, and $\mathbf{a}_{0,i} \in \mathbb{R}^{3 \times 1}$ denote the position bias relative to the 1st PD in the initial position. Since the orientation of the UE may change, let $\mathbf{R} \in \mathbb{R}^{3 \times 3}$ denote the rotation matrix of the UE, and the orientation of the ith PD can be expressed as $\mathbf{n}_i = \mathbf{R}\mathbf{n}_{0,i}$. Hence, after the rotation, the position of the ith PD is given as

$$\mathbf{u}_i = \mathbf{u}_1 + \mathbf{a}_i, i \in \mathcal{K}, \tag{1}$$

where $\mathbf{a}_i = \mathbf{R}\mathbf{a}_{0,i}$ denotes the position bias of the ith PD.

A. Integrated Waveform Design

In this paper, we aim to realize the positioning and communication functions simultaneously via the integrated signal waveform. Let s denote the return-to-zero (RZ) OOK modulation signal with 2 real values q_1 and q_2 with probabilities p_1 and p_2, respectively, such that

$$\mathrm{Pr}\,\{s = q_1\} = p_1, \mathrm{Pr}\,\{s = q_2\} = p_2, p_1 + p_2 = 1. \tag{2}$$

Then, the transmitted signal x is given as

$$x = \sqrt{P}s + I_{\mathrm{DC}}. \tag{3}$$

Since the transmitted signal from the LED is non-negative, we have $\sqrt{P} \leq I_{\text{DC}}$. Moreover, considering the intensity limit of the light, the optical power should be constrained, i.e. $\sqrt{P} \leq P_{\text{p}} - I_{\text{DC}}$, where P_{p} represents the maximum optical power. Combining the signal power and the DC bias power, the total electric power of the transmitted signal x can be expressed by

$$P_e = P_{\text{AC}} + P_{\text{DC}}, \tag{4}$$

where $P_{\text{AC}} = P$ and $P_{\text{DC}} = I_{\text{DC}}^2$ are the electric power of the communication signal and the DC bias, respectively. Hence, the two components can be embedded in x, and transmitted at the same time.

B. Channel Model

Let $\mathbf{h} \triangleq [h_1, \cdots, h_K]^{\text{T}}$ denote the channel gain vector between the lamp and the UE, where h_i is the channel gain between the lamp and the ith PD, including both the LOS link and the the reflection channel. More specifically, according to the VLC channel model [28], [29], h_i is given as

$$h_i = h_{\text{L},i} + h_{\text{d},i}, i \in \mathcal{K}, \tag{5}$$

where $h_{\text{L},i}$ and $h_{\text{d},i}$ denote the gains of the LOS channel and the reflection channel, respectively. The LOS channel gain $h_{\text{L},i}$ is given by [30]

$$h_{\text{L},i} = \frac{(m+1) A_{\text{PD},i}}{2\pi d_i^2} g_{\text{f}} \cos^m (\phi_i) \cos (\psi_i) \operatorname{rect} \left(\frac{\psi_i}{\Psi_c} \right), \tag{6}$$

where m is the Lambertian order, $A_{\text{PD},i}$ represents the receiving area of the ith PD, g_{f} is the gain of the optical concentrator, d_i denotes the distance between the lamp and the ith PD, ϕ_i represents the angle between the emitted light and the normal vector of the lamp, ψ_i is the angle between the emitted light and the normal vector of the ith PD, and Ψ_c stands for FOV of PD. The parameter $\operatorname{rect} (\psi_i / \Psi_c)$ is defined by

$$\operatorname{rect} \left(\frac{\psi_i}{\Psi_c} \right) = \begin{cases} 1, & 0 \leq \psi_i \leq \Psi_c \\ 0, & \text{else} \end{cases}, i \in \mathcal{K}. \tag{7}$$

Since $\mathbf{u}_i = \mathbf{u}_1 + \mathbf{a}_i$, $h_{\text{L},i}$ can be re-expressed as

$$h_{\text{L},i} = \frac{(m+1) A_{\text{PD},i} g_{\text{f}} (\vartheta_3 - \theta_{3,i})^m (\mathbf{u}_{\text{L}} - (\mathbf{u}_1 + \mathbf{a}_i))^{\text{T}} \mathbf{n}_i}{2\pi \|\mathbf{u}_{\text{L}} - (\mathbf{u}_1 + \mathbf{a}_i)\|^{m+3} \|\mathbf{n}_i\|}. \tag{8}$$

For the reflection channel, define $D_{\text{PD},i}$ as the distance between the reflection point and the ith PD, and $D_{\text{BS},i}$ as the distance between the lamp and the reflection point. The reflection channel $h_{\text{d},i}$ is given by [28] and [29]

$$h_{\text{d},i} = \int_{\text{wall}} \left(\frac{\rho (m+1) A_{\text{PD},i}}{2\pi D_{\text{PD},i}^2 D_{\text{BS},i}^2} \cos^m (\phi_i) \cos (\omega_{1,i}) \right. \\ \left. \times \cos (\omega_{2,i}) g_{of} (\psi_i) g_{oc} (\psi_i) \cos (\psi_i) \right) dA_{\text{wall}}, \tag{9}$$

where dA_{wall} represents the reflection area, ρ denotes the reflection coefficient, $g_{of} (\psi_i)$ is the gain of the optical filter and $g_{oc} (\psi_i)$ represents the gain of the optical concentrator. $\omega_{1,i}$ and $\omega_{2,i}$ are the incident angle and the reflection angle of the normal vector of the reflection point, respectively.

For convenience, the channel gain $\mathbf{h}$ of the UE can be expressed as

$$\mathbf{h} = \mathbf{h}_{\text{L}} + \mathbf{h}_{\text{d}}, \tag{10}$$

where $\mathbf{h}_{\text{L}} \triangleq [h_{\text{L},1}, \cdots, h_{\text{L},K}]^{\text{T}}$ and $\mathbf{h}_{\text{d}} \triangleq [h_{\text{d},1}, \cdots, h_{\text{d},K}]^{\text{T}}$ denote the LOS channel and the reflection channel, respectively.

C. Received Signal Model

At the receiver side, we utilize the DC component of the received signal for positioning and the AC component for communication. The existing RSS-based VLP works usually utilize AC for positioning [31], [32]. Specifically, the AC component is received by using PDs, and then the UE's position can be estimated by exploiting the relationship between the visible light channel and the PD's positioning. However, AC positioning usually requires additional frequency band or time slot resources to transmit positioning signals, which will reduce energy efficiency. Note that, in traditional VLC designs, the DC component is only used to ensure that the transmitted signal is non-negative, and is always directly filtered out. In contrast, we exploit the DC component to estimate the UE's position, which can significantly improve the energy efficiency. Specifically, the DC component $\mathbf{y}_{\text{DC}}$ and the AC component $\mathbf{y}_{\text{AC}}$ of the UE are, respectively, given by

$$\mathbf{y}_{\text{DC}} \triangleq [y_{\text{DC},1}, \ldots, y_{\text{DC},K}]^{\text{T}} = \mathbb{E} \{\mathbf{y}\}, \tag{11a}$$

$$\mathbf{y}_{\text{AC}} \triangleq [y_{\text{AC},1}, \ldots, y_{\text{AC},K}]^{\text{T}} = \mathbf{y} - \mathbf{y}_{\text{DC}}, \tag{11b}$$

where $y_{\text{DC},i}$ and $y_{\text{AC},i}$ denote the DC and AC components of the ith PD, respectively.

Based on the channel model, $\mathbf{y}_{\text{DC}}$ and $\mathbf{y}_{\text{AC}}$ can also be expressed as

$$\mathbf{y}_{\text{DC}} = \mathbf{h} I_{\text{DC}} + \mathbf{z}_1, \tag{12a}$$

$$\mathbf{y}_{\text{AC}} = \mathbf{h} \sqrt{P} s + \mathbf{z}_2, \tag{12b}$$

where $\mathbf{z}_1 \triangleq [z_{1,1}, \cdots, z_{1,K}]^{\text{T}}$ and $\mathbf{z}_2 \triangleq [z_{2,1}, \cdots, z_{2,K}]^{\text{T}}$ respectively denote the additive noise in the DC and AC component, respectively. Furthermore, the ith elements in $\mathbf{z}_1$ and $\mathbf{z}_2$ are distributed as $z_{1,i} \sim \mathcal{N} (0, \sigma_i^2), i \in \mathcal{K}$ and $z_{2,i} \sim \mathcal{N} (0, \sigma_i^2), i \in \mathcal{K}$, respectively. Next, we will describe the positioning and communication schemes.

III. POSITIONING SCHEME

A. RSS Positioning Scheme

We exploit the DC component of the received signals of the multiple PDs to estimate the UE's position. According to (12a), the corresponding DC power of $y_{\text{DC},i}$ is given as

$$P_{\text{DC},i} = (h_{\text{L},i} + h_{\text{d},i})^2 I_{\text{DC}}^2 + \sigma_i^2. \tag{13}$$

Furthermore, from (13), $h_{\text{L},i}$ can be rewritten as

$$h_{\text{L},i} = \frac{\sqrt{P_{\text{DC},i} - \sigma_i^2}}{I_{\text{DC}}} - h_{\text{d},i}, i \in \mathcal{K}. \tag{14}$$

Combining the LOS channel model in (8) with (14), we get (15), shown at the bottom of the next page.

Since $i \in \mathcal{K}$, there are K equations and the UE's position $\mathbf{u}_1$ can be calculated. Nonetheless, since these equations include K unknown variables $\{h_{\mathrm{d},i}\}_{i=1}^K$ and one unknown UE's position vector variable $\mathbf{u}_1$, the K equations are under-determined, and there are infinite solutions.

To obtain a high-quality solution, we reduce the number of variables by approximation. Note that the reflection channel gain is much smaller than the LOS channel gain, and the distance between PDs is also small. Thus, we approximate the K reflection channel gains to be equal, i.e. $h_{\mathrm{d},i} = h_{\mathrm{d}}, \forall i \in \mathcal{K}$. Thus, we can obtain K equations given by (16), shown at the bottom of the next page.

To calculate the solutions of the equations in (16), we introduce some auxiliary variables as follows:

$$\boldsymbol{\chi} \triangleq \left[\mathbf{u}_1^{\mathrm{T}}, h_{\mathrm{d}}\right]^{\mathrm{T}}, \tag{17a}$$

$$r_i(\boldsymbol{\chi}) \triangleq \frac{\sqrt{P_{\mathrm{DC},i} - \sigma_i^2}}{I_{\mathrm{DC}}} - h_{\mathrm{d}}$$
$$- \frac{(m+1) A_{\mathrm{PD},i} g_{\mathrm{f}}(\vartheta_3 - \theta_{3,i})^m}{2\pi \|\mathbf{u}_{\mathrm{L}} - (\mathbf{u}_1 + \mathbf{a}_i)\|^{m+3} \|\mathbf{n}_i\|}$$
$$\times \frac{(\mathbf{u}_{\mathrm{L}} - (\mathbf{u}_1 + \mathbf{a}_i))^{\mathrm{T}} \mathbf{n}_i}{2\pi \|\mathbf{u}_{\mathrm{L}} - (\mathbf{u}_1 + \mathbf{a}_i)\|^{m+3} \|\mathbf{n}_i\|}, \tag{17b}$$

$$\mathbf{r}(\boldsymbol{\chi}) \triangleq \left[r_1(\boldsymbol{\chi}), \ldots, r_K(\boldsymbol{\chi})\right]^{\mathrm{T}}. \tag{17c}$$

Then, the equations in (16) can be equivalently reformulated as the NLS optimization problem

$$\min_{\boldsymbol{\chi}} \; f(\boldsymbol{\chi}) = \frac{1}{2} \|\mathbf{r}(\boldsymbol{\chi})\|^2. \tag{18}$$

Here, we propose a modified Newton positioning method to iteratively solve the NLS problem in (18). Specifically, the $(i+1)$th iteration point $\boldsymbol{\chi}^{[i+1]}$ is updated as

$$\boldsymbol{\chi}^{[i+1]} = \boldsymbol{\chi}^{[i]} + \alpha_i \boldsymbol{\delta}^{[i]}, \tag{19}$$

where α_i denotes the step-size of the ith iteration, and $\boldsymbol{\delta}^{[i]} \in \mathbb{R}^{(K+1)\times 1}$ denotes the descending direction of the ith iteration.

The descending direction $\boldsymbol{\delta}^{[i]}$ satisfies the following equation:

$$\nabla^2 f\left(\boldsymbol{\chi}^{[i]}\right) \boldsymbol{\delta}^{[i]} = -\nabla f\left(\boldsymbol{\chi}^{[i]}\right), \tag{20}$$

where $\nabla f\left(\boldsymbol{\chi}^{[i]}\right)$ and $\nabla^2 f\left(\boldsymbol{\chi}^{[i]}\right)$ denote the gradient and the Hessian matrix of $f\left(\boldsymbol{\chi}^{[i]}\right)$, respectively.

To choose a proper step size with a sufficient decrease, we calculate the step-size α_i by the Armijo-Wolfe rule [33], i.e.,

$$f\left(\boldsymbol{\chi}^{[i]} + \alpha_i \boldsymbol{\delta}^{[i]}\right) \leq f\left(\boldsymbol{\chi}^{[i]}\right) + \xi_1 \alpha_i \nabla f\left(\boldsymbol{\chi}^{[i]}\right)^{\mathrm{T}} \boldsymbol{\delta}^{[i]}, \tag{21a}$$

$$\nabla f\left(\boldsymbol{\chi}^{[i]} + \alpha_i \boldsymbol{\delta}^{[i]}\right)^{\mathrm{T}} \boldsymbol{\delta}^{[i]} \geq \xi_2 \nabla f\left(\boldsymbol{\chi}^{[i]}\right)^{\mathrm{T}} \boldsymbol{\delta}^{[i]}, \tag{21b}$$

where $\xi_1, \xi_2 \in (0,1)$ are given parameters, and $\xi_1 < \xi_2$.

In summary, the proposed modified Newton algorithm is listed in Algorithm 1. Based on Algorithm 1, the UE's estimated location $\hat{\mathbf{u}}_1 = [\hat{\theta}_{1,1}, \hat{\theta}_{2,1}, \hat{\theta}_{3,1}]^{\mathrm{T}}$ and the estimated

---

Algorithm 1 The Proposed Modified Newton Positioning Algorithm

Input: Initialize $\boldsymbol{\chi}^{[0]}$, $\alpha_0 = 1$, $i = 0$. Set the convergence tolerance $0 < \mu < 1$;
1: **repeat**
2:      Calculate $\mathbf{r}\left(\boldsymbol{\chi}^{[i]}\right)$, the Jacobian matrix $\mathbf{J}\left(\boldsymbol{\chi}^{[i]}\right)$ and the Hessian matrix $\nabla^2 r_i\left(\boldsymbol{\chi}^{[i]}\right)$;
3:      Calculate the descending direction $\boldsymbol{\delta}^{[i]}$ from (20);
4:      Calculate the step-size α_i using the Armijo-Wolfe rule from (21);
5:      Update $\boldsymbol{\chi}^{[i+1]}$ using (19);
6:      $i \leftarrow i + 1$;
7: **until** $\frac{\left\|\boldsymbol{\chi}^{[i]} - \boldsymbol{\chi}^{[i-1]}\right\|}{\left\|\boldsymbol{\chi}^{[i]}\right\|} \leq \mu$;

Output: $\boldsymbol{\chi}^{[i]}$.

---

value of the reflection channel gain $\hat{h}_{\mathrm{d}}$ can be obtained as follows

$$\left[\hat{\mathbf{u}}_1^{\mathrm{T}}, \hat{h}_{\mathrm{d}}\right]^{\mathrm{T}} = \boldsymbol{\chi}^{[i]}. \tag{22}$$

Next, we will analyze the theoretical bound of the VLP errors based on the CRLB.

B. Positioning Evaluation

Let $\mathbf{u}_1 = [\theta_{1,1}, \theta_{2,1}, \theta_{3,1}]^{\mathrm{T}}$ denote the exact position of the UE, which can be expressed in terms of the estimated position $\hat{\mathbf{u}}_1$ and the positioning error $\mathbf{e}$ as follows

$$\mathbf{u}_1 = \hat{\mathbf{u}}_1 + \mathbf{e}, \tag{23}$$

where $\mathbf{e} = [e_{\mathrm{x}}, e_{\mathrm{y}}, e_{\mathrm{z}}]^{\mathrm{T}}$ represents the positioning error.

Based on (12a), the Fisher information matrix (FIM) $\mathbf{I}_{\mathrm{F}}(\mathbf{u}_1) \in \mathbb{R}^{3\times 3}$ is given by

$$[\mathbf{I}_{\mathrm{F}}(\mathbf{u}_1)]_{j,k} = -\mathbb{E}\left[\frac{\partial^2 \ln p(\mathbf{y}_{\mathrm{DC}}; \mathbf{u}_1)}{\partial \theta_{j,1} \partial \theta_{k,1}}\right], \tag{24}$$

where $\mathbb{E}[\cdot]$ represents the expectation of $p(\mathbf{y}_{\mathrm{DC}}, \mathbf{u}_1)$ and $j = 1, 2, 3$, $k = 1, 2, 3$. $\ln p(\mathbf{y}_{\mathrm{DC}}; \mathbf{u}_1)$ is the corresponding Log-likelihood function which is given by

$$\ln p(\mathbf{y}_{\mathrm{DC}}, \mathbf{u}_1) = -\frac{1}{2\sigma^2} \sum_{i=1}^K \sum_{n=0}^T \left(y_{\mathrm{DC},i} - (h_{\mathrm{L},i} + h_{\mathrm{d},i}) I_{\mathrm{DC}}\right)^2$$
$$- K \ln\left(\sqrt{2\pi}\sigma\right). \tag{25}$$

where T denotes the number of symbols transmitted in each positioning interval.

Let $\mathbf{n}_i = [n_{x,i}, n_{y,i}, n_{z,i}]^{\mathrm{T}}$ denote the normal vector of the ith PD. Then, according to the geometric model shown in Fig. 1, the LOS channel gain of the ith PD can be re-expressed as

$$h_{\mathrm{L},i} = \frac{(m+1) A_{\mathrm{PD},i} g_{\mathrm{f}}(\vartheta_3 - \theta_{3,i})^m \mathbf{d}_i^{\mathrm{T}} \mathbf{n}_i}{2\pi d_i^{m+3} \|\mathbf{n}_i\|} \tag{26a}$$
$$= \frac{(n_{x,i}(\vartheta_1 - \theta_{1,i}) + n_{y,i}(\vartheta_2 - \theta_{2,i}) + n_{z,i}(\vartheta_3 - \theta_{3,i}))}{2\pi \|\mathbf{d}_i\|^{m+3}}$$
$$\times \frac{(m+1) A_{\mathrm{PD},i} g_{\mathrm{f}}(\vartheta_3 - \theta_{3,i})^m}{2\pi \|\mathbf{d}_i\|^{m+3}}, \tag{26b}$$

where $\mathbf{d}_i = [(\vartheta_1 - \theta_{1,i}), (\vartheta_2 - \theta_{2,i}), (\vartheta_3 - \theta_{3,i})]^{\mathrm{T}}$ denotes the vector pointing from the position of the ith PD to the position of the lamp.

Then, the first and second derivative of the log-likelihood function are, respectively, given by

$$\frac{\partial \ln p\left(\mathbf{y}_{\mathrm{DC}}, \mathbf{u}_1\right)}{\partial \theta_{j,1}} = -\frac{1}{\sigma^2} \sum_{i=1}^K \sum_{n=0}^T \left(h_{\mathrm{L},i} I_{\mathrm{DC}}^2 \frac{\partial h_{\mathrm{L},i}}{\partial \theta_{j,1}} \right.$$
$$\left. - y_{\mathrm{DC},i} I_{\mathrm{DC}} \frac{\partial h_{\mathrm{L},i}}{\partial \theta_{j,1}} + h_{\mathrm{d},i} I_{\mathrm{DC}}^2 \frac{\partial h_{\mathrm{L},i}}{\partial \theta_{j,1}} \right), \tag{27a}$$

$$\frac{\partial^2 \ln p\left(\mathbf{y}_{\mathrm{DC}}, \mathbf{u}_1\right)}{\partial \theta_{j,1} \partial \theta_{k,1}} = -\frac{1}{\sigma^2} \sum_{i=1}^K \left(T I_{\mathrm{DC}}^2 \frac{\partial h_{\mathrm{L},i}}{\partial \theta_{j,1}} \frac{\partial h_{\mathrm{L},i}}{\partial \theta_{k,1}} \right.$$
$$\left. - \sum_{n=0}^T z_i I_{\mathrm{DC}} \frac{\partial^2 h_{\mathrm{L},i}}{\partial \theta_{j,1} \partial \theta_{k,1}} \right), \tag{27b}$$

where $\theta_{k,1}$ denotes the kth element of $\mathbf{u}_1$. The expectation to the second derivative of the log-likelihood function is given by

$$\mathbb{E}\left[\frac{\partial^2 \ln p\left(\mathbf{y}_{\mathrm{DC}}; \mathbf{u}_1\right)}{\partial \theta_{j,1} \partial \theta_{k,1}} \right] = -\frac{T}{\sigma^2} \sum_{i=1}^M I_{\mathrm{DC}}^2 \frac{\partial h_{\mathrm{L},i}}{\partial \theta_{j,1}} \frac{\partial h_{\mathrm{L},i}}{\partial \theta_{k,1}}. \tag{28a}$$

According to the CRLB [34], the unbiased estimation of $\mathbf{u}_1$ satisfies

$$\operatorname{var}\left(\hat{\theta}_{j,1} \right) \geq \left[\mathbf{I}_{\mathrm{F}}^{-1}\left(\mathbf{u}_1 \right) \right]_{j,j}, \quad j = 1, 2, 3. \tag{29}$$

Therefore, the positioning error $\mathbf{e}$ satisfies

$$\mathbb{E}\left[\|\mathbf{e}\|^2 \right] \geq \operatorname{Tr}\left(\mathbf{I}_{\mathrm{F}}^{-1} \right), \tag{30}$$

where the FIM $\mathbf{I}_{\mathrm{F}}$ is given by

$$\mathbf{I}_{\mathrm{F}} = \gamma \begin{pmatrix} \sum_{i=1}^K \frac{\partial h_{\mathrm{L},i}}{\partial \theta_{1,1}} \frac{\partial h_{\mathrm{L},i}}{\partial \theta_{1,1}} & \sum_{i=1}^K \frac{\partial h_{\mathrm{L},i}}{\partial \theta_{1,1}} \frac{\partial h_{\mathrm{L},i}}{\partial \theta_{2,1}} & \sum_{i=1}^K \frac{\partial h_{\mathrm{L},i}}{\partial \theta_{1,1}} \frac{\partial h_{\mathrm{L},i}}{\partial \theta_{3,1}} \\ \sum_{i=1}^K \frac{\partial h_{\mathrm{L},i}}{\partial \theta_{2,1}} \frac{\partial h_{\mathrm{L},i}}{\partial \theta_{1,1}} & \sum_{i=1}^K \frac{\partial h_{\mathrm{L},i}}{\partial \theta_{2,1}} \frac{\partial h_{\mathrm{L},i}}{\partial \theta_{2,1}} & \sum_{i=1}^K \frac{\partial h_{\mathrm{L},i}}{\partial \theta_{2,1}} \frac{\partial h_{\mathrm{L},i}}{\partial \theta_{3,1}} \\ \sum_{i=1}^K \frac{\partial h_{\mathrm{L},i}}{\partial \theta_{3,1}} \frac{\partial h_{\mathrm{L},i}}{\partial \theta_{1,1}} & \sum_{i=1}^K \frac{\partial h_{\mathrm{L},i}}{\partial \theta_{3,1}} \frac{\partial h_{\mathrm{L},i}}{\partial \theta_{2,1}} & \sum_{i=1}^K \frac{\partial h_{\mathrm{L},i}}{\partial \theta_{3,1}} \frac{\partial h_{\mathrm{L},i}}{\partial \theta_{3,1}} \end{pmatrix}, \tag{31}$$

where $\gamma = \frac{T I_{\mathrm{DC}}^2}{\sigma^2}$. The first derivatives $\frac{\partial h_{\mathrm{L},i}}{\partial \theta_{1,1}}$, $\frac{\partial h_{\mathrm{L},i}}{\partial \theta_{2,1}}$ and $\frac{\partial h_{\mathrm{L},i}}{\partial \theta_{3,1}}$ are, respectively, given by

$$\frac{\partial h_{\mathrm{L},i}}{\partial \theta_{1,1}} = \kappa_i (\vartheta_3 - \theta_{3,i})^m \left(\mathbf{n}_i^{\mathrm{T}} \mathbf{d}_i \frac{(m+3)(\vartheta_1 - \theta_{1,i})}{\|\mathbf{d}_i\|^{m+5}} \right.$$
$$\left. - \frac{n_{x,i}}{\|\mathbf{d}_i\|^{m+3}} \right), \tag{32a}$$

$$\frac{\partial h_{\mathrm{L},i}}{\partial \theta_{2,1}} = \kappa_i (\vartheta_3 - \theta_{3,i})^m \left(\mathbf{n}_i^{\mathrm{T}} \mathbf{d}_i \frac{(m+3)(\vartheta_2 - \theta_{2,i})}{\|\mathbf{d}_i\|^{m+5}} \right.$$
$$\left. - \frac{n_{y,i}}{\|\mathbf{d}_i\|^{m+3}} \right), \tag{32b}$$

$$\frac{\partial h_{\mathrm{L},i}}{\partial \theta_{3,1}} = \kappa_i \mathbf{n}_i^{\mathrm{T}} \mathbf{d}_i \left(\frac{(m+3)(\vartheta_3 - \theta_{3,i})^{m+1}}{\|\mathbf{d}_i\|^{m+5}} \right.$$
$$\left. - \frac{m(\vartheta_3 - \theta_{3,i})^{m-1}}{\|\mathbf{d}_i\|^{m+3}} \right) - \kappa_i n_{z,i} \frac{(\vartheta_3 - \theta_{3,i})^m}{\|\mathbf{d}_i\|^{m+3}}, \tag{32c}$$

where $\kappa_i = \frac{(m+1) A_{\mathrm{PD},i} g_{\mathrm{f}}}{2\pi}$.

The computed CRLB is a theoretical measure for the positioning error, which will be used in the waveform design optimization of the integrated VLPC system. We will further discuss the waveform optimization problem that involves this CRLB in Section V.

IV. COMMUNICATION SCHEME

A. Effects of Positioning Error

According to the channel model in (6) and (9), the CSI of VLC is a deterministic function of the UE's location. Therefore, the positioning information of the UE can be used for VLC channel estimation. Let $\hat{\mathbf{h}} \triangleq \left[\hat{h}_1, \cdots, \hat{h}_K \right]^{\mathrm{T}}$ and $\Delta\mathbf{h} \triangleq [\Delta h_1, \cdots, \Delta h_K]^{\mathrm{T}}$ denote the estimated CSI and CSI error, respectively, where $\hat{h}_i = \hat{h}_{\mathrm{L},i} + \hat{h}_{\mathrm{d},i}$ and $\Delta h_i = \Delta h_{\mathrm{L},i} + \Delta h_{\mathrm{d},i}$ denote the CSI and estimated CSI error of the ith PD, respectively. Thus, we have

$$\mathbf{h} = \hat{\mathbf{h}} + \Delta\mathbf{h}. \tag{33}$$

In fact, since $\Delta h_{\mathrm{d},i} \ll \Delta h_{\mathrm{L},i}$, the error of the reflection channel can be ignored, i.e., $\Delta h_{\mathrm{d},i} \approx 0$. Based on the channel model in (8), the estimated LOS channel gain of the ith PD

$$\frac{\sqrt{P_{\mathrm{DC},i} - \sigma_i^2}}{I_{\mathrm{DC}}} - h_{\mathrm{d},i} = \frac{(m+1) A_{\mathrm{PD},i} g_{\mathrm{f}} (\vartheta_3 - \theta_{3,i})^m (\mathbf{u}_{\mathrm{L}} - (\mathbf{u}_1 + \mathbf{a}_i))^{\mathrm{T}} \mathbf{n}_i}{2\pi \|\mathbf{u}_{\mathrm{L}} - (\mathbf{u}_1 + \mathbf{a}_i)\|^{m+3} \|\mathbf{n}_i\|}. \tag{15}$$

$$\begin{cases} \frac{\sqrt{P_{\mathrm{DC},1} - \sigma_1^2}}{I_{\mathrm{DC}}} - h_{\mathrm{d}} = \frac{(m+1) A_{\mathrm{PD},1} g_{\mathrm{f}} (\vartheta_3 - \theta_{3,1})^m (\mathbf{u}_{\mathrm{L}} - \mathbf{u}_1)^{\mathrm{T}} \mathbf{n}_1}{2\pi \|\mathbf{u}_{\mathrm{L}} - \mathbf{u}_1\|^{m+3} \|\mathbf{n}_1\|} \\ \frac{\sqrt{P_{\mathrm{DC},2} - \sigma_2^2}}{I_{\mathrm{DC}}} - h_{\mathrm{d}} = \frac{(m+1) A_{\mathrm{PD},2} g_{\mathrm{f}} (\vartheta_3 - \theta_{3,2})^m (\mathbf{u}_{\mathrm{L}} - (\mathbf{u}_1 + \mathbf{a}_2))^{\mathrm{T}} \mathbf{n}_2}{2\pi \|\mathbf{u}_{\mathrm{L}} - (\mathbf{u}_1 + \mathbf{a}_2)\|^{m+3} \|\mathbf{n}_2\|} \\ \quad\quad\quad \vdots \\ \frac{\sqrt{P_{\mathrm{DC},K} - \sigma_K^2}}{I_{\mathrm{DC}}} - h_{\mathrm{d}} = \frac{(m+1) A_{\mathrm{PD},K} g_{\mathrm{f}} (\vartheta_3 - \theta_{3,K})^m (\mathbf{u}_{\mathrm{L}} - (\mathbf{u}_1 + \mathbf{a}_K))^{\mathrm{T}} \mathbf{n}_K}{2\pi \|\mathbf{u}_{\mathrm{L}} - (\mathbf{u}_1 + \mathbf{a}_K)\|^{m+3} \|\mathbf{n}_K\|} \end{cases} \tag{16}$$

$\hat{h}_{\mathrm{L},i}$ is given by

$$\hat{h}_{\mathrm{L},i} = \frac{\kappa_i(\vartheta_3 - \theta_{3,i})^m (\mathbf{u}_{\mathrm{L}} - (\hat{\mathbf{u}}_1 + \mathbf{a}_i))^{\mathrm{T}} \mathbf{n}_i}{\|\mathbf{u}_{\mathrm{L}} - (\hat{\mathbf{u}}_1 + \mathbf{a}_i)\|^{m+3}}, \qquad (34a)$$

Here, we assume that the normal vectors of all PDs are unit vectors, i.e., $\|\mathbf{n}_i\| = 1, i \in \mathcal{K}$. We assume that the positioning error follows a Gaussian distribution, i.e., $\mathbf{e} \sim \mathcal{N}\left(\mathbf{0}, \mathbf{I}_{\mathrm{FIM}}^{-1}(I_{\mathrm{DC}})\right)$ [35], [36]. Furthermore, for the ith PD, the CSI error function of the UE's location errors is given by

$$\Delta h_i(\mathbf{e})$$
$$= h_i - \hat{h}_i \qquad (35a)$$
$$= \frac{\kappa_i\left(\vartheta_3 - \left(\hat{\theta}_{3,i} + e_z\right)\right)^m (\mathbf{u}_{\mathrm{L}} - (\hat{\mathbf{u}}_1 + \mathbf{a}_i + \mathbf{e}))^{\mathrm{T}} \mathbf{n}_i}{\|\mathbf{u}_{\mathrm{L}} - (\hat{\mathbf{u}}_1 + \mathbf{a}_i + \mathbf{e})\|^{m+3}}$$
$$- \frac{\kappa_i\left(\vartheta_3 - \hat{\theta}_{3,i}\right)^m (\mathbf{u}_{\mathrm{L}} - (\hat{\mathbf{u}}_1 + \mathbf{a}_i))^{\mathrm{T}} \mathbf{n}_i}{\|\mathbf{u}_{\mathrm{L}} - (\hat{\mathbf{u}}_1 + \mathbf{a}_i)\|^{m+3}}. \qquad (35b)$$

Therefore, the mean of Δh_i is given by

$$\mathbb{E}[\Delta h_i] = \int \Delta h_i(\mathbf{e}) f_{\mathrm{PDF}}(\mathbf{e})\, d\mathbf{e}, \qquad (36)$$

where $f_{\mathrm{PDF}}(\mathbf{e})$ is the probability density function (PDF) of $\mathbf{e}$.

Then, the mean of $\Delta \mathbf{h}$ is given as $\mathbb{E}[\Delta \mathbf{h}] = [\mathbb{E}[\Delta h_1], \cdots, \mathbb{E}[\Delta h_K]]^{\mathrm{T}}$. Let $\mathbb{D}[\Delta \mathbf{h}]$ denote the covariance matrix of $\Delta \mathbf{h}$, where $[\mathbb{D}[\Delta \mathbf{h}]]_{m,n}$ represents the element in the mth row and nth column. Furthermore, $[\mathbb{D}[\Delta \mathbf{h}]]_{m,n}$ is given as

$$[\mathbb{D}[\Delta \mathbf{h}]]_{m,n} = \mathbb{E}\left[(\Delta h_m - \mathbb{E}[\Delta h_m])(\Delta h_n - \mathbb{E}[\Delta h_n])\right]. \qquad (37)$$

Let $\mathcal{P}$ denote the distribution set with mean $\mathbb{E}[\Delta \mathbf{h}]$ and covariance $\mathbb{D}[\Delta \mathbf{h}]$, i.e.,

$$\mathcal{P} \triangleq \{\mathbb{P}_{\mathbf{x}} | \mathbf{x} \sim \mathbb{P}_{\mathbf{x}}, \mathbb{E}[\mathbf{x}] = \mathbb{E}[\Delta \mathbf{h}], \mathbb{D}[\mathbf{x}] = \mathbb{D}[\Delta \mathbf{h}]\}, \qquad (38)$$

where $\mathbf{x} \sim \mathbb{P}_{\mathbf{x}}$ indicates that the random variable $\mathbf{x}$ follows the distribution of $\mathbb{P}_{\mathbf{x}}$. Obviously, $\Delta \mathbf{h} \sim \mathbb{P}_{\Delta \mathbf{h}}$ and $\mathbb{P}_{\Delta \mathbf{h}} \in \mathcal{P}$.

B. Achievable Rate Expressions

Since there are K PDs at the UE, we apply receive beamforming at the K PDs, which is denoted as $\mathbf{w} = [w_1, \cdots, w_K]^{\mathrm{T}} \in \mathbb{R}^{K \times 1}$. Moreover, the magnitude of $\mathbf{w}$ is 1, i.e., $\|\mathbf{w}\| = 1$. By applying this beamformer to the received signals $\{y_{\mathrm{AC},i}\}_{i=1}^{K}$, we have

$$y_{\mathrm{AC}} = \mathbf{w}^{\mathrm{T}} \mathbf{h} \sqrt{P} s + \mathbf{w}^{\mathrm{T}} \mathbf{z}_2, \qquad (39)$$

where $\mathbf{z}_2 = [z_{2,1}, \cdots, z_{2,K}]^{\mathrm{T}} \in \mathbb{R}^{K \times 1}$ represents the additive white Gaussian noise (AWGN) vector, and $\mathbf{w}^{\mathrm{T}} \mathbf{z}_2$ obeys a Gaussian distribution with a mean of 0 and a variance of σ^2, i.e., $\mathbf{w}^{\mathrm{T}} \mathbf{z}_2 \sim \mathcal{N}(0, \sigma^2)$.

Thus, the PDF $f_Y(y_{\mathrm{AC}})$ of the received signal y_{AC} at the UE is given as

$$f_Y(y_{\mathrm{AC}}) = \sum_{n=1}^{2} \frac{p_n}{\sqrt{2\pi}\sigma} e^{-\frac{\left(y_{\mathrm{AC}} - \mathbf{w}^{\mathrm{T}} \mathbf{h} \sqrt{P} q_n\right)^2}{2\sigma^2}}. \qquad (40)$$

Furthermore, based on the OOK signal inputs, the VLC achievable rate is given by

$$R(\Delta \mathbf{h}) = I(s; y_{\mathrm{AC}}) \qquad (41a)$$

$$= -\frac{1}{2\ln 2} - \sum_{n=1}^{2} p_n E_{\mathbf{w}^{\mathrm{T}} \mathbf{z}_2} \left[\log_2 \sum_{m=1}^{2} \left(p_m \right. \right.$$
$$\left. \left. \times e^{-\frac{\left(\mathbf{w}^{\mathrm{T}}(\hat{\mathbf{h}} + \Delta \mathbf{h})\sqrt{P}(q_n - q_m) + \mathbf{w}^{\mathrm{T}} \mathbf{z}_2\right)^2}{2\sigma^2}} \right) \right]. \qquad (41b)$$

The detailed derivations for (41) are given in Appendix 41. According to (A), the achievable rate of VLC R is a function of the discrete OOK constellation points $\{q_n\}_{n=1}^{2}$ and the corresponding probabilities $\{p_n\}_{n=1}^{2}$. However, the achievable rate (41b) is not in a closed-form expression, and thus the calculation of (41b) is computationally inefficient. To reduce the computational complexity, we further derive an analytical expression for its lower bound. Specifically, the lower bound of the achievable rate (41b) is given by (see Appendix B for the derivation)

$$R_{\mathrm{L}}(\Delta \mathbf{h}) = -\sum_{n=1}^{2} p_n \log_2 \sum_{m=1}^{2} p_m e^{-\frac{\left(\mathbf{w}^{\mathrm{T}}(\hat{\mathbf{h}} + \Delta \mathbf{h})\sqrt{P}(q_n - q_m)\right)^2}{4\sigma^2}}$$
$$- \frac{1 - \ln 2}{2\ln 2}. \qquad (42)$$

For brevity, the detailed derivations for (42) are listed in Appendix B. When the probability of OOK signals satisfies $p_1 = p_2 = 0.5$ and the VLPC bandwidth is B_{VLPC} (Hz), the lower bound of the achievable rate of OOK signal reduces to

$$R_{\mathrm{L}}(\Delta \mathbf{h}) = -2B_{\mathrm{VLPC}} \log_2 \left(e^{-\frac{\left(\mathbf{w}^{\mathrm{T}}(\hat{\mathbf{h}} + \Delta \mathbf{h})\sqrt{P}\right)^2}{4B_{\mathrm{VLPC}}\sigma^2}} + 1 \right)$$
$$- \frac{(1 - 3\ln 2)B_{\mathrm{VLPC}}}{2\ln 2}. \qquad (43)$$

According to (43), the rate lower bound of OOK signals is a function of the CSI error $\Delta \mathbf{h}$, which is also random. Therefore, we adopt the outage probability in the waveform optimization of the VLPC system.

V. INTEGRATED WAVEFORM OPTIMIZATION

Based on the proposed waveform design principle, we further optimize the DC and AC components and receiver beamformer to minimize the positioning error CRLB, while satisfying the total transmit power constraint and the outage probability of communication rate. Mathematically, the integrated waveform optimization problem can be formulated as

$$\min_{\mathbf{w}, P, I_{\mathrm{DC}}} \quad \mathrm{Tr}\left(\mathbf{I}_{\mathrm{F}}^{-1}(I_{\mathrm{DC}})\right) \qquad (44a)$$

$$\text{s.t.} \quad P + I_{\mathrm{DC}}^2 \leq P_{\mathrm{total}}, \qquad (44b)$$

$$\inf_{\mathbb{P}_{\Delta \mathbf{h}} \in \mathcal{P}} \mathrm{Pr}\left\{R_{\mathrm{L}}(\Delta \mathbf{h}) \geq \tilde{R}\right\} \leq 1 - p_{\mathrm{out}}, \qquad (44c)$$

$$\sqrt{P} \leq I_{\mathrm{DC}}, \qquad (44d)$$

$$\Delta \mathbf{h} \sim \mathbb{P}_{\Delta \mathbf{h}}, \qquad (44e)$$

where P_{total} denotes the threshold of the total transmit power, $\tilde{R}$ denotes the rate threshold of the VLPC system, and p_{out} represents the maximum tolerable outage probability. Problem (44) is non-convex and difficult to solve. The main challenge is that constraint (44c) is a probabilistic constraint, and does not have a closed-form expression.

To overcome this challenge, we transform the optimization problem into a tractable form. By defining auxiliary variables $\hat{\mathbf{w}} \triangleq \sqrt{P}\mathbf{w}$ and $\hat{P}_{\text{I}} \triangleq I_{\text{DC}}^2$, problem (44) can be equivalently reformulated as

$$\min_{\hat{\mathbf{w}}, \hat{P}_{\text{I}}} \quad \text{Tr}\left(\mathbf{I}_{\text{F}}^{-1}\left(\hat{P}_{\text{I}}\right)\right) \tag{45a}$$

$$\text{s.t. } \|\hat{\mathbf{w}}\|^2 + \hat{P}_{\text{I}} \le P_{\text{total}}, \tag{45b}$$

$$\|\hat{\mathbf{w}}\|^2 \le \hat{P}_{\text{I}}, \tag{45c}$$

$$(44c), (44e).$$

Let $\hat{\mathbf{W}} = \hat{\mathbf{w}}\hat{\mathbf{w}}^{\text{T}}$, and $\hat{\mathbf{W}} \in \mathbb{R}^{K \times K}$ satisfy $\text{rank}\left(\hat{\mathbf{W}}\right) = 1$, $\hat{\mathbf{W}} \succeq \mathbf{0}$. Based on the Semidefinite Relaxation (SDR) method and ignoring the constraint $\text{rank}\left(\hat{\mathbf{W}}\right) = 1$, (45) can be equivalently expressed as

$$\min_{\hat{\mathbf{W}}, \hat{P}_{\text{I}}} \quad \text{Tr}\left(\mathbf{I}_{\text{F}}^{-1}\left(\hat{P}_{\text{I}}\right)\right) \tag{46a}$$

$$\text{s.t. } \text{Tr}\left(\hat{\mathbf{W}}\right) + \hat{P}_{\text{I}} \le P_{\text{total}}, \tag{46b}$$

$$\text{Tr}\left(\hat{\mathbf{W}}\right) \le \hat{P}_{\text{I}}, \hat{\mathbf{W}} \succeq \mathbf{0}, \tag{46c}$$

$$(44c), (44e).$$

Then, $R_{\text{L}}\left(\Delta\mathbf{h}\right) \ge \tilde{R}$ in (44c) can be equivalently written as

$$-\Delta\mathbf{h}^{\text{T}}\hat{\mathbf{W}}\Delta\mathbf{h} - 2\hat{\mathbf{h}}^{\text{T}}\hat{\mathbf{W}}\Delta\mathbf{h} - \hat{\mathbf{h}}^{\text{T}}\tilde{\mathbf{W}}\hat{\mathbf{h}} - \varpi \le 0, \tag{47}$$

where $\varpi = 4\sigma^2 \ln\left(2^{-\frac{1-3\ln 2}{2\ln 2} - \tilde{R}} - 1\right)$. Thus, (44c) can be equivalently expressed as follows

$$\inf_{\mathbb{P}_{\Delta\mathbf{h}} \in \mathcal{P}} \quad \text{Pr}\left\{-\Delta\mathbf{h}^{\text{T}}\hat{\mathbf{W}}\Delta\mathbf{h} - 2\hat{\mathbf{h}}^{\text{T}}\hat{\mathbf{W}}\Delta\mathbf{h} - \hat{\mathbf{h}}^{\text{T}}\hat{\mathbf{W}}\hat{\mathbf{h}} - \varpi \le 0\right\}$$
$$\ge 1 - p_{\text{out}}, \tag{48}$$

where $\inf_{\mathbb{P}_{\Delta\mathbf{h}} \in \mathcal{P}}$ represents the lower bound of the probability when the probability distribution is $\mathbb{P}_{\Delta\mathbf{h}}$. The ambiguity set is denoted by $\mathcal{P}$, which includes all channel error distributions.

Lemma 1: [37], [38] For a continuous loss function $L: \mathbb{R}_k \to \mathbb{R}$, which is concave or quadratic in $\mathbf{X}$, the distributionally robust chance constraint is equivalent to the worst-case constraint, i.e.,

$$\inf_{\mathbb{P} \in \mathcal{P}} \text{Pr}_{\mathbb{P}}\left\{L\left(\boldsymbol{\eta}\right) \le 0\right\} \ge 1 - \lambda$$
$$\Leftrightarrow \sup_{\mathbb{P} \in \mathcal{P}} \mathbb{P} - \text{CVaR}_\lambda\left\{L\left(\boldsymbol{\eta}\right)\right\} \le 0, \tag{49}$$

where $\mathbb{P} - \text{CVaR}_\lambda\left\{L\left(\boldsymbol{\eta}\right)\right\}$ is the CVaR of $L\left(\boldsymbol{\eta}\right)$ with respect to $\mathbb{P}$ under threshold λ, i.e.,

$$\mathbb{P} - \text{CVaR}_\lambda\left\{L\left(\boldsymbol{\eta}\right)\right\} = \inf_{\beta \in \mathbb{R}}\left\{\beta + \frac{1}{\lambda}\mathbb{E}_{\mathbb{P}}\left[\left(L\left(\boldsymbol{\eta}\right) - \beta\right)^+\right]\right\}, \tag{50}$$

where $\mathbb{R}$ denotes the real numbers set and $(a)^+ \triangleq \max\{0, a\}$.

Lemma 2: [37], [38] Let $L\left(\boldsymbol{\eta}\right) = \boldsymbol{\eta}^{\text{T}}\boldsymbol{V}\boldsymbol{\eta} + \mathbf{v}^{\text{T}}\boldsymbol{\eta} + v_0$ be a quadratic function of $\boldsymbol{\eta}, \forall\boldsymbol{\eta} \in \mathbb{R}^n$. The worst-case CVaR is given by

$$\sup_{\mathbb{P} \in \mathcal{P}} \mathbb{P} - \text{CVaR}_\lambda\left\{L\left(\boldsymbol{\eta}\right)\right\} = \min_{\beta, \mathbf{M}} \beta + \frac{1}{\lambda}\text{Tr}\left(\boldsymbol{\Omega}\mathbf{M}\right) \tag{51a}$$

$$\text{s.t. } \mathbf{M} \in \mathbb{S}^{n+1}, \beta \in \mathbb{R}, \mathbf{M} \succeq \mathbf{0}, \tag{51b}$$

$$\mathbf{M} - \begin{bmatrix} \boldsymbol{V} & \frac{\mathbf{v}}{2} \\ \frac{\mathbf{v}^{\text{T}}}{2} & v_0 - \beta \end{bmatrix} \succeq \mathbf{0}, \tag{51c}$$

where $\mathbf{M}$ and β are the auxiliary variables and $\boldsymbol{\Omega}$ is given by

$$\boldsymbol{\Omega} \triangleq \begin{bmatrix} \boldsymbol{\Sigma} + \boldsymbol{\mu}\boldsymbol{\mu}^{\text{T}} & \boldsymbol{\mu} \\ \boldsymbol{\mu}^{\text{T}} & 1 \end{bmatrix}, \tag{52}$$

where $\boldsymbol{\mu} \in \mathbb{R}^n$ and $\boldsymbol{\Sigma} \in \mathbb{S}^n$ are the mean vector and covariance matrix of vector $\boldsymbol{\eta}$, respectively.

Based on Lemma 1 and Lemma 2, we introduce a quadratic function $L\left(\Delta\mathbf{h}\right) \triangleq -\Delta\mathbf{h}^{\text{T}}\hat{\mathbf{W}}\Delta\mathbf{h} - 2\hat{\mathbf{h}}^{\text{T}}\hat{\mathbf{W}}\Delta\mathbf{h} - \hat{\mathbf{h}}^{\text{T}}\tilde{\mathbf{W}}\hat{\mathbf{h}} - \varpi$, and then constraint (48) can be conservatively approximated by the worst-case CVaR constraint, i.e.,

$$\begin{cases} \beta + \dfrac{1}{p_{\text{out}}}\text{Tr}\left(\boldsymbol{\Omega}\mathbf{M}\right) \le 0, \\ \mathbf{M} \in \mathbb{S}^{K+1}, \beta \in \mathbb{R}, \mathbf{M} \succeq \mathbf{0}, \\ \mathbf{M} + \begin{bmatrix} \hat{\mathbf{W}} & \hat{\mathbf{W}}^{\text{T}}\hat{\mathbf{h}} \\ \hat{\mathbf{h}}^{\text{T}}\hat{\mathbf{W}} & \hat{\mathbf{h}}^{\text{T}}\tilde{\mathbf{W}}\hat{\mathbf{h}} + \varpi + \beta \end{bmatrix} \succeq \mathbf{0}, \end{cases} \tag{53}$$

where $\mathbf{M}$ and β denote two auxiliary varibles and $\boldsymbol{\Omega}$ is defined as

$$\boldsymbol{\Omega} \triangleq \begin{bmatrix} \mathbb{D}\left[\Delta\mathbf{h}\right] + \mathbb{E}\left[\Delta\mathbf{h}\right]\mathbb{E}[\Delta\mathbf{h}]^{\text{T}} & \mathbb{E}\left[\Delta\mathbf{h}\right] \\ \mathbb{E}[\Delta\mathbf{h}]^{\text{T}} & 1 \end{bmatrix}. \tag{54}$$

Then, the constrained problem (46) can be formulated as follows

$$\min_{\hat{\mathbf{W}}, \hat{P}_{\text{I}}, \mathbf{M}, \beta} \quad \text{Tr}\left(\mathbf{I}_{\text{F}}^{-1}\left(\hat{P}_{\text{I}}\right)\right) \tag{55a}$$

$$\text{s.t. } \text{Tr}\left(\hat{\mathbf{W}}\right) + \hat{P}_{\text{I}} \le P_{\text{total}}, \tag{55b}$$

$$\text{Tr}\left(\hat{\mathbf{W}}\right) \le \hat{P}_{\text{I}}, \tag{55c}$$

$$\hat{\mathbf{W}} \succeq \mathbf{0}, \tag{55d}$$

$$\beta + \frac{1}{p_{\text{out}}}\text{Tr}\left(\boldsymbol{\Omega}\mathbf{M}\right) \le 0, \tag{55e}$$

$$\mathbf{M} \in \mathbb{S}^{K+1}, \beta \in \mathbb{R}, \mathbf{M} \succeq \mathbf{0}, \tag{55f}$$

$$\mathbf{M} + \begin{bmatrix} \hat{\mathbf{W}} & \hat{\mathbf{W}}^{\text{T}}\hat{\mathbf{h}} \\ \hat{\mathbf{h}}^{\text{T}}\hat{\mathbf{W}} & \hat{\mathbf{h}}^{\text{T}}\tilde{\mathbf{W}}\hat{\mathbf{h}} + \varpi + \beta \end{bmatrix} \succeq \mathbf{0}. \tag{55g}$$

Unfortunately, the variables $\mathbf{M}$ and $\boldsymbol{\Omega}$ are coupled in constraint (55e), and thus problem (55) is non-convex and intractable. To overcome this challenge, we exploit the BCD algorithm [39] to deal with the non-convexity and non-separability in (55). Furthermore, problem (55) can be efficiently solved by alternately updating two variable blocks, i.e., optimizing $\left\{\hat{\mathbf{W}}, \mathbf{M}, \beta\right\}$ in the VLC sub-problem and $\left\{\hat{P}_{\text{I}}\right\}$ in the VLP sub-problem.

Algorithm 2 BCD Algorithm for the Optimal Integrated Waveform Design

---
Input: Initialize $\hat{P}_{\mathrm{I}}^{[0]} = \frac{P_{\mathrm{total}}}{2}$, the maximum iterations number $N_{\max}$ and the convergence tolerance $\xi > 0$. Set $k = 0$;
1: **repeat**
2: Update $\left\{ \hat{\mathbf{W}}^{[k+1]}, \mathbf{M}^{[k+1]}, \beta^{[k+1]}, \varepsilon^{[k+1]} \right\}$ by solving VLC subproblem (56) with fixed $\left\{ \hat{P}_{\mathrm{I}}^{[k]} \right\}$;
3: Update $\left\{ \hat{P}_{\mathrm{I}}^{[k+1]} \right\}$ by solving VLP subproblem (57) with fixed $\left\{ \hat{\mathbf{W}}^{[k+1]} \right\}$;
4: $k \leftarrow k + 1$;
5: **until** $\left| \frac{\mathrm{Tr}\left(\mathbf{I}_{\mathrm{F}}^{-1}\left(\hat{P}_{\mathrm{I}}^{[k]} \right) \right) - \mathrm{Tr}\left(\mathbf{I}_{\mathrm{F}}^{-1}\left(\hat{P}_{\mathrm{I}}^{[k-1]} \right) \right)}{\mathrm{Tr}\left(\mathbf{I}_{\mathrm{F}}^{-1}\left(\hat{P}_{\mathrm{I}}^{[k]} \right) \right)} \right| \leq \xi$ or $k > N_{\max}$;

Output: $\hat{P}_{\mathrm{I}}^{[k]}$ and $\hat{\mathbf{W}}^{[k]}$.

---

1) VLC Sub-Problem: For the given variable block $\left\{ \hat{P}_{\mathrm{I}} \right\}$, the variables $\left\{ \hat{\mathbf{W}}, \mathbf{M}, \beta \right\}$ can be solved by the VLC sub-problem as follows:

$$\min_{\hat{\mathbf{W}}, \mathbf{M}, \beta} \quad \mathrm{Tr}\left(\hat{\mathbf{W}} \right)$$
$$\text{s.t.} \quad (55b), (55c), (55d), (55e), (55f), (55g), \qquad (56)$$

which is convex and can be solved using the interior point methods, such as CVX [40].

2) VLP Sub-Problem: For the given variable block $\left\{ \hat{\mathbf{W}} \right\}$, the variable $\left\{ \hat{P}_{\mathrm{I}} \right\}$ can be solved by the VLP sub-problem as follows:

$$\min_{\hat{P}_{\mathrm{I}}} \quad \mathrm{Tr}\left(\mathbf{I}_{\mathrm{F}}^{-1}\left(\hat{P}_{\mathrm{I}} \right) \right)$$
$$\text{s.t.} \quad (55b), (55c), \qquad (57)$$

which is convex. Since constraint (55e) is intractable, it is relaxed in the VLP sub-problem.

In summary, the BCD algorithm for the optimal integrated waveform design is listed in Algorithm 2. Since both sub-problems are convex, Algorithm 2 can globally converge to the set of Karush-Kuhn-Tucker (KKT) points of problem (55). The complexity of the BCD algorithm is $\mathcal{O}\left(k^{-1} \right)$, where k is the index of iteration [41]. Moreover, the worst case complexity of the two SDP problem are $\mathcal{O}\left(\max\{m, n\}^4 n^{0.5} \log \xi^{-1} \right)$, where m denotes the number of constraints, n denotes the problem size and ξ is the convergence tolerance of the SDP problem [42]. Note that, due to the SDR, the rank of the output solution $\hat{\mathbf{W}}^{[k]}$ may not be 1. When $\mathrm{rank}\left(\hat{\mathbf{W}}^{[k]} \right) = 1$, the optimal receiving beamformer $\hat{\mathbf{w}}$ is obtained by the eigenvalue decomposition (EVD) of $\hat{\mathbf{W}}^{[k]}$. Otherwise, a high quality feasible solution $\hat{\mathbf{w}}$ can be calculated by Gaussian randomization [42]. The solutions P, $\mathbf{w}$ and I_{DC} of the original problem (44) can be expressed as $P = \|\hat{\mathbf{w}}\|^2$, $\mathbf{w} = \frac{\hat{\mathbf{w}}}{\sqrt{P}}$ and $I_{\mathrm{DC}} = \sqrt{\hat{P}_{\mathrm{I}}^{[k]}}$, respectively.

VI. SIMULATION RESULTS AND DISCUSSIONS

We consider a VLPC system with a single LED lamp in a $(4 \times 4 \times 3.5)$ room. The center of the ceiling is the origin $[0, 0, 0]^{\mathrm{T}}$ of the Cartesian coordinate system. Moreover, the positions of the LED is $[0, 0, 0]^{\mathrm{T}}$ and the PD normals are assumed to be all vertically up, i.e., $\mathbf{n}_i = [0, 0, 1]^{\mathrm{T}}, \forall i \in \mathcal{K}$. It is assumed that there are K PDs on the UE device, and the

TABLE II
SIMULATION PARAMETERS

Parameter	Value
FOV Ψ_c	$90°$
Lambertian order m	1
PD's physical receiving area A_{PD}	$1\mathrm{cm}^2$
The gain of the optical concentrator g_{f}	1
VLPC bandwidth B_{VLPC}	$20\mathrm{MHz}$
Power spectral density of noise N_0	$10^{-21}\mathrm{A}^2/\mathrm{Hz}$
The number of symbols T	200

placement of the PDs is as follows: $K - 1$ PDs are located at the vertices of the regular $K - 1$ polygon, one PD is located at the centroid of the regular $K - 1$ polygon which is the location of UE, and the distance between the PDs on the vertices and the PD at the centroid is L_{PD}. The detailed simulation parameters are given in Table II.

A. Positioning Scheme

In this section, we will analyze the positioning performance through simulations. It is worth noting that the CRLB represents the mean square value of the positioning error. For convenience, we use the root mean square error (RMSE) $r_{\mathrm{e}} \triangleq \sqrt{\mathbb{E}\left[\|\mathbf{e}\|_2^2 \right]}$ to represent the positioning error. In addition, we compare the proposed modified Newton positioning algorithm with the CRLB and the maximum likelihood estimation (MLE) algorithm.

Fig. 2(a) shows the positioning error of Newton versus the vertical distance between the UE and lamp for different positioning power levels. It can be seen that the positioning error of Newton increases with the increase of vertical distance. Fig. 2(b) depicts the positioning error of Newton versus the horizontal distance between the UE and lamp for different positioning power levels. As the horizontal distance increases, the positioning error increases. Whether the vertical distance or the horizontal distance increases, the received signal power at the UE is reduced. Then, the received signal-to-noise ratio (SNR) decreases, and the positioning error increases. In addition, it can also be seen that higher positioning power, results in higher positioning accuracy.

Fig. 3 depicts the positioning error of Newton versus the vertical L_{PD} for different positioning power levels where the location of the UE $\mathbf{u}_1 = [0, 0, -2]^{\mathrm{T}}$. We can observe that an increase in L_{PD} decreases the positioning error. Since the increase of L_{PD} enlarges the difference in received power between different PDs, it is more helpful to identify the positioning information of the UE. However, for an actual system, the trade-off between the size of the receiver and the positioning function needs to be weighed.

Fig. 4 depicts the positioning error r_{e} versus the number of PDs K and the DC power, where $L_{\mathrm{PD}} = 0.1\mathrm{m}$ and the UE is $\mathbf{u}_1 = [-1, -1, -1]^{\mathrm{T}}$. From Fig. 4, we observe that as the number of receiver PDs increases, the positioning error decreases. The reason is that the increase of the number of PDs
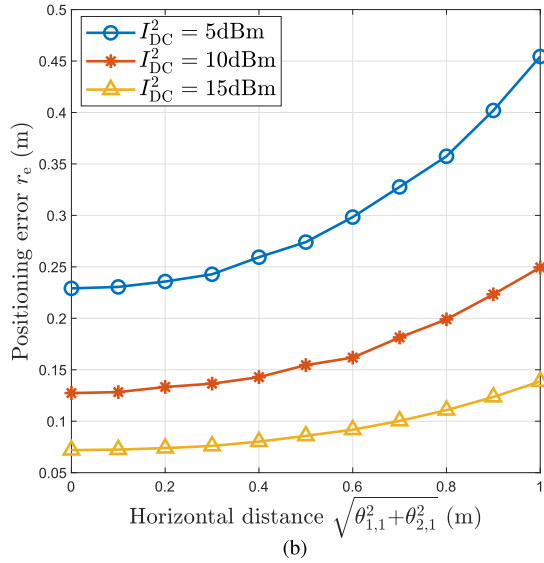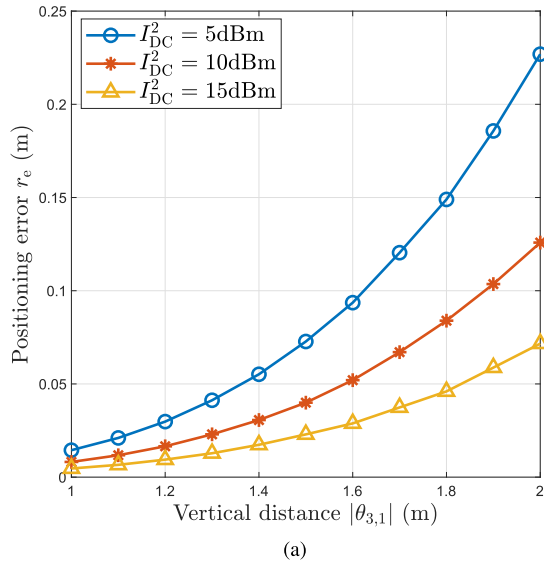
(a)

(b)

Fig. 2. (a) Position error versus vertical distance $|\theta_{3,1}|$; (b) Position error versus horizontal distance $\sqrt{\theta_{1,1}^2+\theta_{2,1}^2}$.

Fig. 3. Position error versus distance L_{PD}.

Fig. 4. Positioning error r_{e} versus the number of PDs K.

can provide more spatial location differences of PDs, which is beneficial to improve the positioning accuracy.

Fig. 5 illustrates the relationship between the average positioning error and the DC power where the number of PDs $K = 5$, $L_{\mathrm{PD}} = 0.1\mathrm{m}$ and the UE is $\mathbf{u}_1 = [-1, -1, -1]^{\mathrm{T}}$. It can be seen that for $\sqrt{\mathrm{CRLB}}$, Newton and MLE, the average positioning error decreases with the increase in positioning power. In addition, the positioning error of the Newton algorithm is larger than that of MLE and CRLB and is especially pronounced at lower SNR. This is because CRLB is a theoretical lower bound, and the performance of the Newton algorithm will theoretically be worse than MLE. However, MLE requires a large number of samples, which is not applicable in practical systems. In addition, when the SNR is high, the performance of the Newton algorithm is close to MLE, which makes the Newton algorithm favorable in an actual system due to its lower complexity.

B. Optimal Integrated Waveform Design

To measure the performance of the optimal integrated waveform design, we introduce a non-robust design based on perfect CSI and compare it with our proposed robust design which takes the CSI error $\Delta\mathbf{h}$ into account.

In Fig. 6, we plot the CDFs of the communication rate in the non-robust scenario, the robust scenario with outage probabilities $P_{\mathrm{out}} = 0.05$ and $P_{\mathrm{out}} = 0.15$, and the perfect CSI scenario, where the number of PDs $K = 5$, $L_{\mathrm{PD}} = 0.1\mathrm{m}$, the location of the UE $\mathbf{u}_1 = [-1, -1, -2]^{\mathrm{T}}$, the rate threshold $\tilde{R} = 10\mathrm{Mbit/s}$ and total power $P_{\mathrm{total}} = 0.1W$. It can be seen that the probability that the communication rate is lower than the rate threshold in the non-robust scenario is about 30%, which is far larger than the outage constraint. This poor performance is due to the randomness of imperfect CSI, hence the robust design is required to ensure that the rate meets the outage probability requirement. However, in the robust case, both $P_{\mathrm{out}} = 0.05$ and $P_{\mathrm{out}} = 0.15$ satisfy the requirements of their respective outage probability designs,
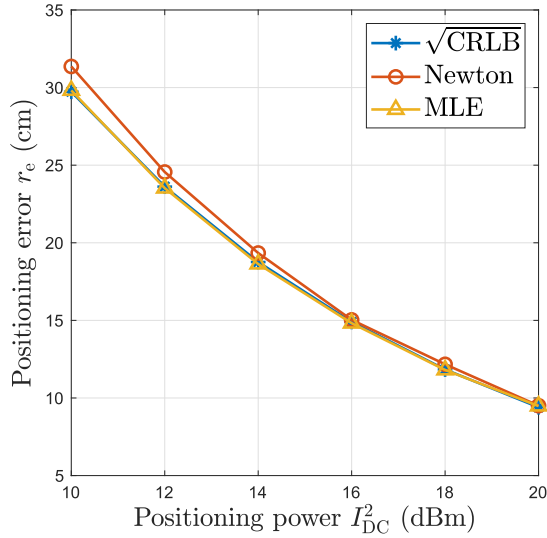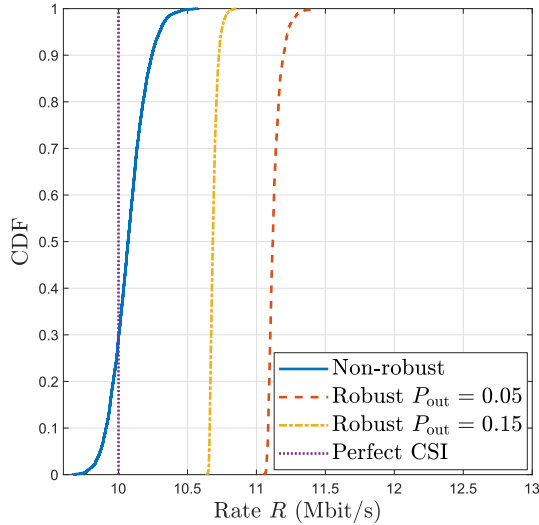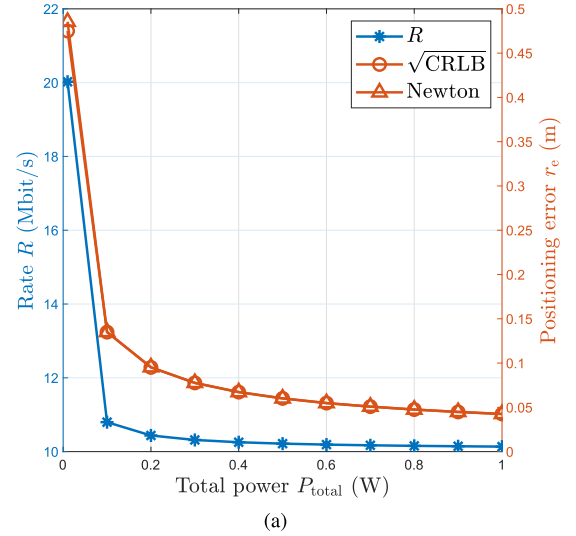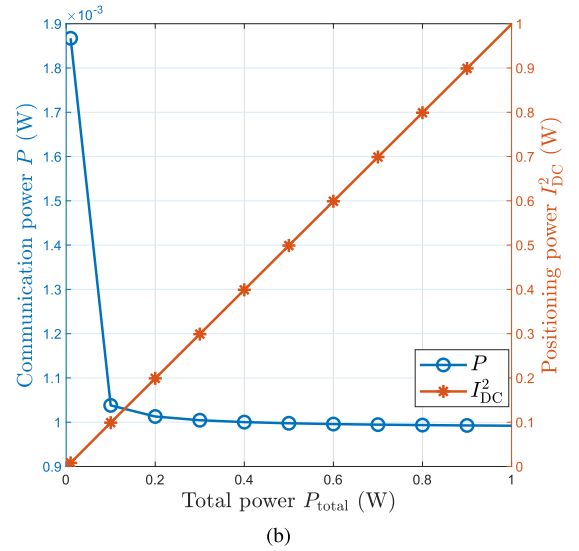
Fig. 5.   Positioning error versus positioning power I_{DC}^2.

Fig. 6.   Comparison of the CDFs of the communication rate R in different CSI situations.

Fig. 7.   (a) Rate R and positioning error of the proposed waveform design versus total power P_{total}; (b) Communication power P and positioning power I_{DC}^2 of the proposed waveform design versus total power P_{total}.

and the design at $P_{\mathrm{out}} = 0.05$ is more conservative than the design at $P_{\mathrm{out}} = 0.15$. Furthermore, the rate in the perfect CSI scenario is exactly equal to the rate threshold. Therefore, Fig. 6 demonstrates the effectiveness of our proposed robust optimal integrated waveform design.

Fig. 7(a) shows the rate R and the positioning error of $\sqrt{\mathrm{CRLB}}$ and Newton of the optimal integrated waveform design versus total power P_{total} where the number of PDs $K = 5$, $L_{\mathrm{PD}} = 0.1\mathrm{m}$, the UE is $\mathbf{u}_1 = [-1, -1, -2]^{\mathrm{T}}$, the rate threshold $\tilde{R} = 10\mathrm{Mbit/s}$ and the outage probability $P_{\mathrm{out}} = 0.1$. It can be seen from Fig. 7(a) that the communication rate R, the positioning error of $\sqrt{\mathrm{CRLB}}$ and Newton all gradually decrease with the increase of the total power P_{total}. In addition, the communication rate R will eventually approach the rate threshold $\tilde{R}$. The improved positioning accuracy reduces the conservativeness of the communication performance, thereby reducing the average communication rate. When the positioning is accurate enough, it can be

regarded as perfect CSI, and thus the rate will tend to the rate threshold. Fig. 7(b) depicts the communication power P and positioning power I_{DC}^2 of the optimal integrated waveform design versus total power P_{total} where the number of PDs $K = 5$, $L_{\mathrm{PD}} = 0.1\mathrm{m}$, the UE is $\mathbf{u}_1 = [-1, -1, -2]^{\mathrm{T}}$, the rate threshold $\tilde{R} = 10\mathrm{Mbit/s}$ and the outage probability $P_{\mathrm{out}} = 0.1$. As the total power increases, the positioning power increases but the communication power decreases. Due to the increase in total power P_{total}, the VLPC system can allocate more power for positioning. The positioning accuracy is proportional to the positioning power, which reduces the conservativeness of communication and the average rate, thereby reducing the power required for communication.

Fig. 8(a) illustrates the rate R and the positioning error of $\sqrt{\mathrm{CRLB}}$ and Newton of the optimal integrated waveform design versus outage probability P_{out} where the number of PDs $K = 5$, $L_{\mathrm{PD}} = 0.1\mathrm{m}$, the location of the UE $\mathbf{u}_1 = [-1, -1, -2]^{\mathrm{T}}$, the total power $P_{\mathrm{total}} = 0.0188\mathrm{W}$ and the rate threshold $\tilde{R} = 10\mathrm{Mbit/s}$. As the outage probability P_{out}
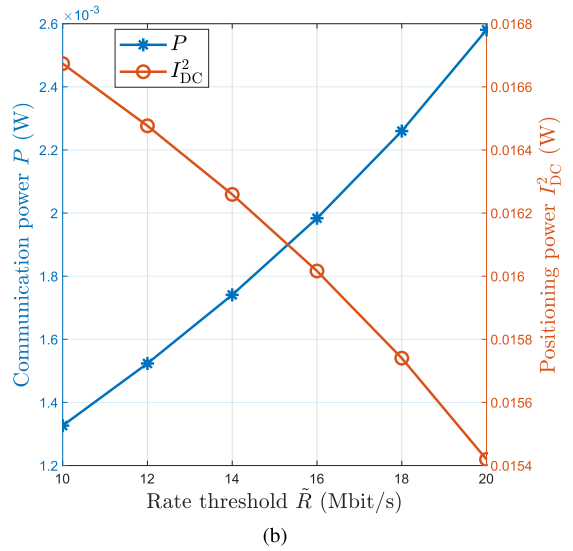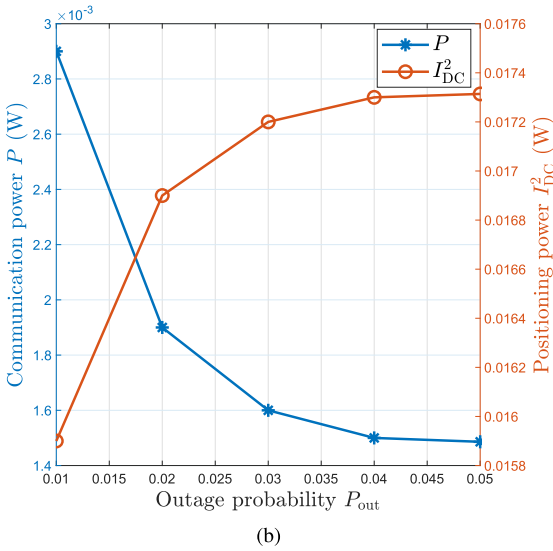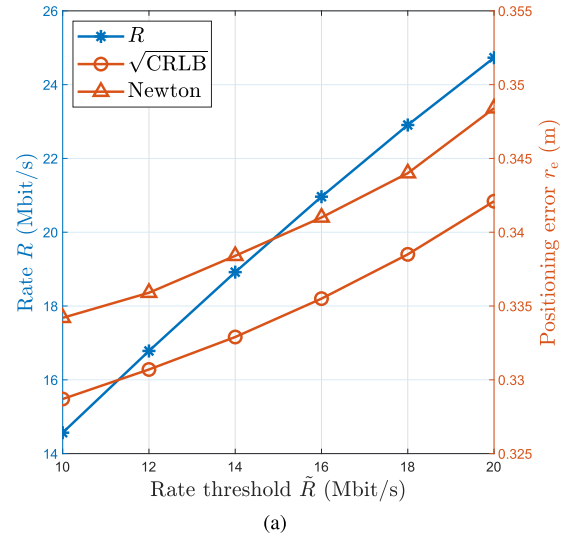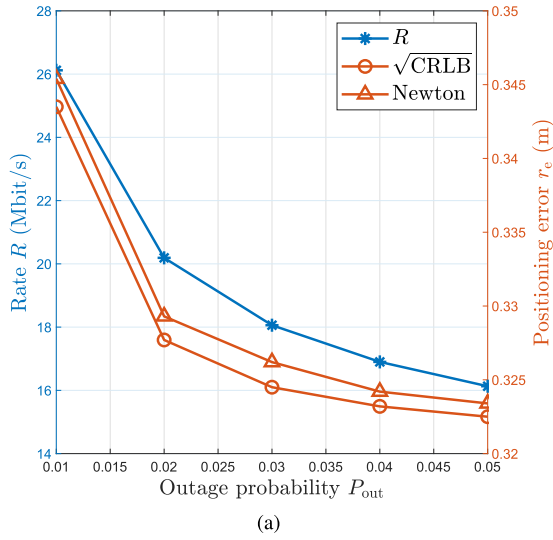
Fig. 8. (a) Rate R and positioning error of the proposed waveform design versus outage probability P_{out}; (b) Communication power P and positioning power I_{DC}^2 of the proposed waveform design versus outage probability P_{out}.

Fig. 9. (a) Rate R and positioning error of the proposed waveform design versus rate threshold $\tilde{R}$; (b) Communication power P and positioning power I_{DC}^2 of the proposed waveform design versus rate threshold $\tilde{R}$.

increases, the communication rate R, the positioning error of $\sqrt{\text{CRLB}}$ and Newton all gradually decrease. Fig. 8(b) depicts communication power P and positioning power I_{DC}^2 of the optimal integrated waveform design versus outage probability P_{out} where the number of PDs $K = 5$, $L_{\text{PD}} = 0.1\text{m}$, the UE is $\mathbf{u}_1 = [-1, -1, -2]^{\text{T}}$, the total power $P_{\text{total}} = 0.0188\text{W}$ and the rate threshold $\tilde{R} = 10\text{Mbit/s}$. We can see that the positioning power increases when the outage probability P_{out} increases. But the communication power decreases as the outage probability P_{out} increases. This is because the increase of the outage probability reduces the conservativeness of the communication, and thus the communication rate decreases accordingly. Then, the communication power is reduced accordingly, so that the positioning power is increased when the total power remains unchanged. Finally, the positioning performance is improved due to the improved positioning power.

Fig. 9(a) depicts the rate R and the positioning error of $\sqrt{\text{CRLB}}$ and Newton of the optimal integrated waveform design versus rate threshold $\tilde{R}$ where the number of PDs $K = 5$, $L_{\text{PD}} = 0.1\text{m}$, the UE is $\mathbf{u}_1 = [-1, -1, -2]^{\text{T}}$, the total power $P_{\text{total}} = 0.018\text{W}$ and the outage probability $P_{\text{out}} = 0.1$. It can be seen from Fig. 9(a) that the communication rate R, the positioning error of $\sqrt{\text{CRLB}}$ and Newton all gradually increase when the rate threshold $\tilde{R}$ increases. Fig. 9(b) illustrates communication power P and positioning power I_{DC}^2 of the optimal integrated waveform design versus rate threshold $\tilde{R}$ where the number of PDs $K = 5$, $L_{\text{PD}} = 0.1\text{m}$, the UE is $\mathbf{u}_1 = [-1, -1, -2]^{\text{T}}$, the total power $P_{\text{total}} = 0.018\text{W}$ and the outage probability $P_{\text{out}} = 0.1$. The positioning power drops with the increase in $\tilde{R}$, but the communication power increases when the rate threshold $\tilde{R}$ increases. Due to the increase of the rate threshold $\tilde{R}$, the rate constraint makes the communication rate increase. With a fixed total rate, more power is allocated to communications. Therefore, the positioning power is relatively reduced, the positioning accuracy is reduced, and the positioning error is increased.
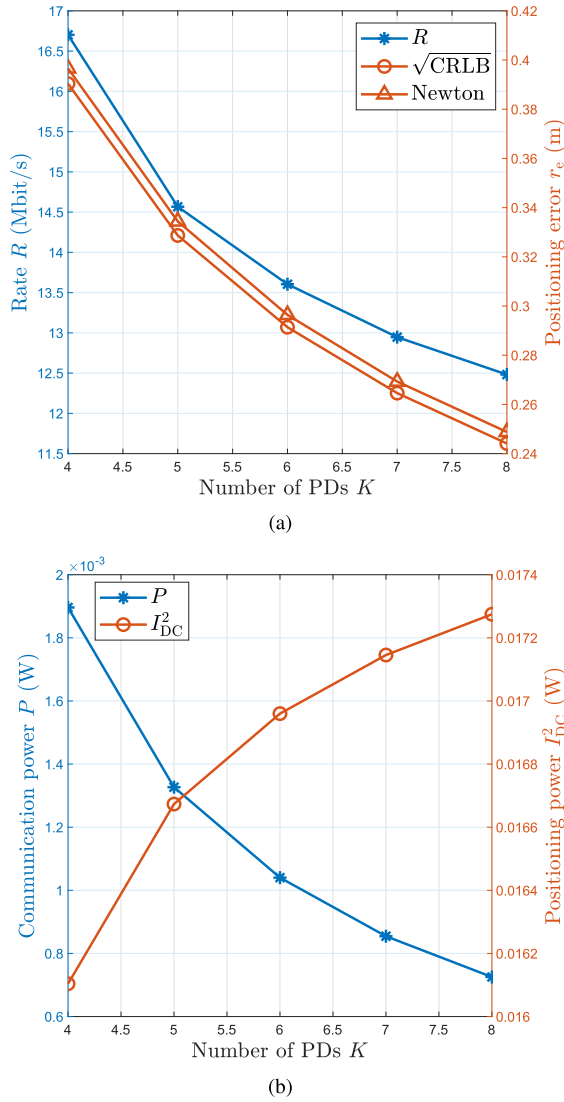
Fig. 10. (a) Rate R and positioning error of the proposed waveform design versus the number of PDs K; (b) Communication power P and positioning power I_{DC}^2 of the proposed waveform design versus the number of PDs K.

Fig. 10(a) shows the rate R and the positioning error of $\sqrt{\text{CRLB}}$ and Newton of the optimal integrated waveform design versus the number of PDs K, where $L_{PD} = 0.1$m, the UE is $\mathbf{u}_1 = [-1, -1, -2]^T$, the total power $P_{total} = 0.018$W, the rate threshold $\tilde{R} = 10$Mbit/s and the outage probability $P_{out} = 0.1$. It can be seen that, as the number of PDs K increases, the communication rate R, the positioning error of $\sqrt{\text{CRLB}}$ and Newton all gradually decrease. Fig. 10(b) depicts the communication power P and positioning power I_{DC}^2 of the optimal integrated waveform design versus the number of PDs K where $L_{PD} = 0.1$m, the UE is $\mathbf{u}_1 = [-1, -1, -2]^T$, the total power $P_{total} = 0.018$W, the rate threshold $\tilde{R} = 10$Mbit/s and the outage probability $P_{out} = 0.1$. We can see that, as K increases, positioning power I_{DC}^2 increases but the communication power P decreases. It is worth noting that when the positioning power is a constant, increasing the number of PDs will improve the positioning accuracy. In our VLPC robust design, the total power remains unchanged. At this time, if the number of PDs is increased and the positioning power remains unchanged, the positioning accuracy will be improved. As the positioning accuracy improves, the communication conservatism will decrease, resulting in a decrease in the communication rate. In return, the power required for communication is reduced, and the positioning power will increase when the total power is a constant.

VII. CONCLUSION

In this work, we proposed an energy efficient waveform design and optimization framework for integrated VLPC systems, where the DC and AC components are used for positioning and communication, respectively. Specifically, for the VLPC system with a single LED, we designed a modified Newton method to iteratively solve the 3D positioning problem, and derived the CRLB expression to analyze positioning performance. Furthermore, based on the fact that the CSI of the LOS link is a deterministic function of the PDs' position and orientation, the positioning results are utilized for CSI estimation of VLC, which can significantly reduce the overhead of the VLPC system. Then, by adopting the BCD algorithm, the optimal waveform design is developed, which minimizes the CRLB and satisfies the outage probability constraint of VLC rate, and the total power constraint. Finally, our simulation results demonstrated both the effectiveness and robustness of the proposed waveform design for VLPC problem.

APPENDIX

A. Derivation of (41)

The derivation of information transmission rate based on OOK $R(\Delta \mathbf{h})$ is given by (58), shown at the top of the next page.

B. Derivation of The Lower Bound (42)

The information transmission rate based on OOK $R(\Delta \mathbf{h})$ is lower bounded by

$R(\Delta \mathbf{h})$

$$\geq -\frac{1}{2\ln 2} - \sum_{n=1}^{2} p_n \log_2 \sum_{m=1}^{2} \left(E_{\mathbf{w}^T \mathbf{z}_2} \left[p_m \right.\right.$$
$$\left.\left. \times e^{-\frac{\left(\mathbf{w}^T \mathbf{h}\sqrt{P}(q_n - q_m) + \mathbf{w}^T \mathbf{z}_2\right)^2}{2\sigma^2}} \right] \right) \tag{59a}$$

$$= -\frac{1}{2\ln 2} - \sum_{n=1}^{2} p_n \log_2 \sum_{m=1}^{2} \left(p_m \int_{-\infty}^{\infty} \frac{1}{\sqrt{2\pi}\sigma} \right.$$
$$\left. \times e^{-\frac{\left(\mathbf{w}^T \mathbf{h}\sqrt{P}(q_n - q_m) + \mathbf{w}^T \mathbf{z}_2\right)^2 + \left(\mathbf{w}^T \mathbf{z}_2\right)^2}{2\sigma^2}} \right) d\mathbf{w}^T \mathbf{z}_2 \tag{59b}$$

$$= -\sum_{n=1}^{2} p_n \log_2 \sum_{m=1}^{2} \frac{p_m}{\sqrt{2}} e^{-\frac{\left(\mathbf{w}^T \mathbf{h}\sqrt{P}(q_n - q_m)\right)^2}{4\sigma^2}} - \frac{1}{2\ln 2} \tag{59c}$$

$$= -\sum_{n=1}^{2} p_n \log_2 \sum_{m=1}^{2} p_m e^{-\frac{\left(\mathbf{w}^T(\hat{\mathbf{h}} + \Delta \mathbf{h})\sqrt{P}(q_n - q_m)\right)^2}{4\sigma^2}}$$
$$- \frac{1 - \ln 2}{2\ln 2}, \tag{59d}$$

$$R\left(\Delta\mathbf{h}\right) = I\left(s; y_{AC}\right) \tag{58a}$$

$$= h\left(y_{AC}\right) - h\left(y_{AC}|s\right) \tag{58b}$$

$$= -\int_{-\infty}^{\infty} f_Y\left(y_{AC}\right)\log_2 f_Y\left(y_{AC}\right) dy_{AC} - \frac{1}{2}\log_2\left(2\pi e\sigma^2\right) \tag{58c}$$

$$= -\frac{1}{2}\log_2\left(2\pi e\sigma^2\right) - \int_{-\infty}^{\infty}\left(\sum_{n=1}^{2}\frac{p_n}{\sqrt{2\pi}\sigma}e^{-\frac{\left(\mathbf{w}^{\mathrm{T}}\mathbf{h}\sqrt{P}q_n + \mathbf{w}^{\mathrm{T}}\mathbf{z}_2 - \mathbf{w}^{\mathrm{T}}\mathbf{h}\sqrt{P}q_n\right)^2}{2\sigma^2}}\right.$$
$$\times \left.\log_2\sum_{m=1}^{2}\frac{p_m}{\sqrt{2\pi}\sigma}e^{-\frac{\left(\mathbf{w}^{\mathrm{T}}\mathbf{h}\sqrt{P}q_n + \mathbf{w}^{\mathrm{T}}\mathbf{z}_2 - \mathbf{w}^{\mathrm{T}}\mathbf{h}\sqrt{P}q_m\right)^2}{2\sigma^2}}\right) d\mathbf{w}^{\mathrm{T}}\mathbf{z}_2 \tag{58d}$$

$$= -\sum_{n=1}^{2}p_n\mathbb{E}_{\mathbf{w}^{\mathrm{T}}\mathbf{z}_2}\left[\log_2\sum_{m=1}^{2}\frac{p_m}{\sqrt{2\pi}\sigma}e^{-\frac{\left(\mathbf{w}^{\mathrm{T}}\mathbf{h}\sqrt{P}(q_n - q_m) + \mathbf{w}^{\mathrm{T}}\mathbf{z}_2\right)^2}{2\sigma^2}}\right] - \frac{1}{2}\log_2\left(2\pi e\sigma^2\right) \tag{58e}$$

$$= -\frac{1}{2\ln 2} - \sum_{n=1}^{2}p_n\mathbb{E}_{\mathbf{w}^{\mathrm{T}}\mathbf{z}_2}\left[\log_2\sum_{m=1}^{2}p_m e^{-\frac{\left(\mathbf{w}^{\mathrm{T}}\mathbf{h}\sqrt{P}(q_n - q_m) + \mathbf{w}^{\mathrm{T}}\mathbf{z}_2\right)^2}{2\sigma^2}}\right] \tag{58f}$$

$$= -\frac{1}{2\ln 2} - \sum_{n=1}^{2}p_n\mathbb{E}_{\mathbf{w}^{\mathrm{T}}\mathbf{z}_2}\left[\log_2\sum_{m=1}^{2}p_m e^{-\frac{\left(\mathbf{w}^{\mathrm{T}}(\hat{\mathbf{h}} + \Delta\mathbf{h})\sqrt{P}(q_n - q_m) + \mathbf{w}^{\mathrm{T}}\mathbf{z}_2\right)^2}{2\sigma^2}}\right]. \tag{58g}$$

where the inequality (59a) holds due to Jensen's Inequality [43].

Therefore, we obtain the lower bound expression $R_{\mathrm{L}}\left(\Delta\mathbf{h}\right)$ as (42).

REFERENCES

[1] A. Jovicic, J. Li, and T. Richardson, "Visible light communication: Opportunities, challenges and the path to market," *IEEE Commun. Mag.*, vol. 51, no. 12, pp. 26–32, Dec. 2013.

[2] N. E. Klepeis et al., "The national human activity pattern survey (NHAPS): A resource for assessing exposure to environmental pollutants," *J. Exposure Sci. Environ. Epidemiol.*, vol. 11, no. 3, pp. 231–252, Jul. 2001.

[3] P. H. Pathak, X. Feng, P. Hu, and P. Mohapatra, "Visible light communication, networking, and sensing: A survey, potential and challenges," *IEEE Commun. Surveys Tuts.*, vol. 17, no. 4, pp. 2047–2077, Sep. 2015.

[4] H. Haas, L. Yin, Y. Wang, and C. Chen, "What is LiFi?" *J. Lightw. Technol.*, vol. 34, no. 6, pp. 1533–1544, Mar. 15, 2016.

[5] W. Xu, J. Wang, H. Shen, H. Zhang, and X. You, "Indoor positioning for multiphotodiode device using visible-light communications," *IEEE Photon. J.*, vol. 8, no. 1, pp. 1–11, Feb. 2016.

[6] B. Li, X. Xue, S. Feng, and W. Xu, "Layered optical OFDM with adaptive bias for dimming compatible visible light communications," *J. Lightw. Technol.*, vol. 39, no. 11, pp. 3434–3444, Jun. 2021.

[7] T. K. Khani, H. B. Mangrio, and F. A. Umrani, "Performance analysis of VLC system using commercially available components," in *Proc. 22nd Int. Multitopic Conf. (INMIC)*, Nov. 2019, pp. 1–4.

[8] S. Ma, Y. He, H. Li, S. Lu, F. Zhang, and S. Li, "Optimal power allocation for mobile users in non-orthogonal multiple access visible light communication networks," *IEEE Trans. Commun.*, vol. 67, no. 3, pp. 2233–2244, Mar. 2019.

[9] X. Ling, J. Wang, X. Liang, Z. Ding, and C. Zhao, "Offset and power optimization for DCO-OFDM in visible light communication systems," *IEEE Trans. Signal Process.*, vol. 64, no. 2, pp. 349–363, Jan. 2016.

[10] Z. Li, H. Yu, B. Shan, D. Zou, and S. Li, "New run-length limited codes in on–off keying visible light communication systems," *IEEE Wireless Commun. Lett.*, vol. 9, no. 2, pp. 148–151, Feb. 2020.

[11] *Visible Light Beacon Systems*, Standard JEITA Standard CP-1223, Mar. 2013.

[12] *IEEE Standard for Local and Metropolitan Area Networks—Part 15.7: Short-Range Wireless Optical Communication Using Visible Light*, Standard IEEE 802.15.7-2011, Sep. 2011, pp. 1–309.

[13] *IEEE Standard for Local and Metropolitan Area Networks—Part 15.7: Short-Range Optical Wireless Communications*, Standard 802.15.7-2018 (Revision of IEEE Std 802.15.7-2011), Apr. 2019, pp. 1–407.

[14] X. Yu, J. Wang, and H. Lu, "Single LED-based indoor positioning system using multiple photodetectors," *IEEE Photon. J.*, vol. 10, no. 6, pp. 1–8, Dec. 2018.

[15] F. Alam, N. Faulkner, M. Legg, and S. Demidenko, "Indoor visible light positioning using spring-relaxation technique in real-world setting," *IEEE Access*, vol. 7, pp. 91347–91359, 2019.

[16] P. Du et al., "Experimental demonstration of 3D visible light positioning using received signal strength with low-complexity trilateration assisted by deep learning technique," *IEEE Access*, vol. 7, pp. 93986–93997, 2019.

[17] T. Akiyama, M. Sugimoto, and H. Hashizume, "Time-of-arrival-based smartphone localization using visible light communication," in *Proc. Int. Conf. Indoor Positioning Indoor Navigat. (IPIN)*, Sep. 2017, pp. 1–7.

[18] C. Amini, A. Taherpour, T. Khattab, and S. Gazor, "Theoretical accuracy analysis of indoor visible light communication positioning system based on time-of-arrival," in *Proc. IEEE Can. Conf. Electr. Comput. Eng. (CCECE)*, May 2016, pp. 1–5.

[19] S. Jung, S. Hann, and C. Park, "TDOA-based optical wireless indoor localization using LED ceiling lamps," *IEEE Trans. Consum. Electron.*, vol. 57, no. 4, pp. 1592–1597, Nov. 2011.

[20] S.-H. Yang, H.-S. Kim, Y.-H. Son, and S.-K. Han, "Three-dimensional visible light indoor localization using AOA and RSS with multiple optical receivers," *J. Lightw. Technol.*, vol. 32, no. 14, pp. 2480–2485, Jul. 1, 2014.

[21] S. De Lausnay, L. De Strycker, J. Goemaere, N. Stevens, and B. Nauwelaers, "A visible light positioning system using frequency division multiple access with square waves," in *Proc. 9th Int. Conf. Signal Process. Commun. Syst. (ICSPCS)*, Dec. 2015, pp. 1–7.

[22] B. Lin, X. Tang, Z. Ghassemlooy, C. Lin, and Y. Li, "Experimental demonstration of an indoor VLC positioning system based on OFDMA," *IEEE Photon. J.*, vol. 9, no. 2, pp. 1–9, Apr. 2017.

[23] Y. Xu et al., "Accuracy analysis and improvement of visible light positioning based on VLC system using orthogonal frequency division multiple access," *Opt. Exp.*, vol. 25, no. 26, Dec. 2017, Art. no. 32618.

[24] H. Yang, C. Chen, W.-D. Zhong, A. Alphones, S. Zhang, and P. Du, "Demonstration of a quasi-gapless integrated visible light communication and positioning system," *IEEE Photon. Technol. Lett.*, vol. 30, no. 23, pp. 2001–2004, Dec. 1, 2018.

[25] H. Yang, W. Zhong, C. Chen, A. Alphones, and P. Du, "QoS-driven optimized design-based integrated visible light communication and positioning for indoor IoT networks," *IEEE Internet Things J.*, vol. 7, no. 1, pp. 269–283, Jan. 2020.

[26] H. Yang, P. Du, W. Zhong, C. Chen, A. Alphones, and S. Zhang, "Reinforcement learning-based intelligent resource allocation for integrated VLCP systems," *IEEE Wireless Commun. Lett.*, vol. 8, no. 4, pp. 1204–1207, Aug. 2019.

[27] H. Yang et al., "Coordinated resource allocation-based integrated visible light communication and positioning systems for indoor IoT," *IEEE Trans. Wireless Commun.*, vol. 19, no. 7, pp. 4671–4684, Jul. 2020.

[28] S. Feng, R. Zhang, W. Xu, and L. Hanzo, "Multiple access design for ultra-dense VLC networks: Orthogonal vs non-orthogonal," *IEEE Trans. Commun.*, vol. 67, no. 3, pp. 2218–2232, Mar. 2019.

[29] R. Zhang, Y. Cui, H. Claussen, H. Haas, and L. Hanzo, "Anticipatory association for indoor visible light communications: Light, follow me!" *IEEE Trans. Wireless Commun.*, vol. 17, no. 4, pp. 2499–2510, Apr. 2018.

[30] M. D. Soltani, Z. Zeng, I. Tavakkolnia, H. Haas, and M. Safari, "Random receiver orientation effect on channel gain in LiFi systems," in *Proc. IEEE Wireless Commun. Netw. Conf. (WCNC)*, Apr. 2019, pp. 1–6.

[31] C. Carreño et al., "Comparison of metaheuristic optimization algorithms for RSS-based 3-D visible light positioning systems," in *Proc. South Amer. Colloq. Visible Light Commun. (SACVC)*, Jun. 2020, pp. 1–6.

[32] S. Zhang, P. Du, C. Chen, W. Zhong, and A. Alphones, "Robust 3D indoor VLP system based on ANN using hybrid RSS/PDOA," *IEEE Access*, vol. 7, pp. 47769–47780, 2019.

[33] J. H. Y. L. Z. Wen and H. Liu., *Optimization: Modeling, Algorithm and Theory*. Beijing, China: Higher Education Press, 2020.

[34] M. F. Keskin, S. Gezici, and O. Arikan, "Direct and two-step positioning in visible light systems," *IEEE Trans. Commun.*, vol. 66, no. 1, pp. 239–254, Jan. 2018.

[35] T. Wang, G. Leus, and L. Huang, "Ranging energy optimization for robust sensor positioning based on semidefinite programming," *IEEE Trans. Signal Process.*, vol. 57, no. 12, pp. 4777–4787, Dec. 2009.

[36] A. D. V. Lottici and U. Mengali, "Channel estimation for ultrawideband communications," *IEEE J. Sel. Areas Commun.*, vol. 20, no. 9, pp. 1638–1645, Dec. 2002.

[37] S. Zymler, D. Kuhn, and B. Rustem, "Distributionally robust joint chance constraints with second-order moment information," *Math. Program.*, vol. 137, nos. 1–2, pp. 167–198, Feb. 2013.

[38] Y. Zhang, B. Li, F. Gao, and Z. Han, "A robust design for ultra reliable ambient backscatter communication systems," *IEEE Internet Things J.*, vol. 6, no. 5, pp. 8989–8999, Oct. 2019.

[39] Y. Wu, W. Yang, X. Guan, and Q. Wu, "UAV-enabled relay communication under malicious jamming: Joint trajectory and transmit power optimization," *IEEE Trans. Veh. Technol.*, vol. 70, no. 8, pp. 8275–8279, Aug. 2021.

[40] M. Grant and S. Boyd. (Mar. 2014). *CVX: MATLAB Software for Disciplined Convex Programming, Version 2.1*. [Online]. Available: http://cvxr.com/cvx

[41] C. Cartis, N. I. M. Gould, and P. L. Toint, "On the complexity of steepest descent, Newton's and regularized Newton's methods for nonconvex unconstrained optimization problems," *SIAM J. Optim.*, vol. 20, no. 6, pp. 2833–2852, Jan. 2010.

[42] Z.-Q. Luo, W.-K. Ma, A. So, Y. Ye, and S. Zhang, "Semidefinite relaxation of quadratic optimization problems," *IEEE Signal Process. Mag.*, vol. 27, no. 3, pp. 20–34, May 2010.

[43] W. Zeng, C. Xiao, and J. Lu, "A low-complexity design of linear precoding for MIMO channels with finite-alphabet inputs," *IEEE Wireless Commun. Lett.*, vol. 1, no. 1, pp. 38–41, Feb. 2012.

Shiyu Cao received the B.S. degree in communication engineering from the Hohai University of Computer and Information Technology, Nanjing, China. He is currently pursuing the M.E. degree in information and communication engineering with the School of Information and Control Engineering, China University of Mining and Technology, Xuzhou, China. His research interests include visible light communication and mechanical antenna.

Hang Li received the B.E. and M.S. degrees from Beihang University, Beijing, China, in 2008 and 2011, respectively, and the Ph.D. degree from Texas A&M University, College Station, TX, USA, in 2016. He was a Post-Doctoral Research Associate with Texas A&M University, from September 2016 to August 2017, and the University of California at Davis, September 2017 to March 2018. From April 2018 to June 2019, he was a Visiting Research Scholar with the Shenzhen Research Institute of Big Data, Shenzhen, China, where he has been a Research Scientist, since June 2019. His current research interests include wireless networks, the Internet of Things, stochastic optimization, and the applications of machine learning.

Songtao Lu (Member, IEEE) received the Ph.D. degree in electrical engineering from Iowa State University in 2018. He was a Post-Doctoral Associate with the Department of Electrical and Computer Engineering, University of Minnesota Twin Cities, from 2018 to 2019, and an AI Resident at the IBM Thomas J. Watson Research Center from 2019 to 2020. Currently, he is a Senior Research Scientist with the Mathematics and Theoretical Computer Science group at the IBM Thomas J. Watson Research Center, Yorktown Heights, NY, USA, and affiliated with the MIT-IBM Watson AI Laboratory, Cambridge, MA, USA. His primary interests are in the areas of signal processing, wireless communications, machine learning, and optimization. He also served as an Area Chair for NeurIPS 2023 and AAAI 2021, 2022, and 2023. He received the Best Paper Runner-Up Award of UAI in 2022, an Outstanding Paper Award from FL-NeurIPS in 2022, an IBM Research Accomplishment Award in 2021, the ICML 2019 and AISTATS 2017 Travel Awards, a Graduate and Professional Student Senate Research Award at Iowa State University in 2017, and a Research Excellence Award from the Graduate College at Iowa State University in 2017.

Shuai Ma (Member, IEEE) received the B.S. and Ph.D. degrees in communication and information systems from Xidian University, Xi'an, China, in 2009 and 2016, respectively. From 2014 to 2015, he was a Visiting Scholar with the Department of Electrical and Computer Engineering, Texas A&M University, College Station, TX, USA. From 2016 to 2019, he was an Associate Professor with the School of Information and Control Engineering, China University of Mining and Technology, Xuzhou, China. From 2019 to 2022, he was a Post-Doctoral Fellow with Télécom Paris, France. Since 2023, he has been an Associate Researcher with the Peng Cheng Laboratory, Shenzhen, China. His research interests include semantic communications, visible light communications, and network information theory.

Tingting Yang received the Ph.D. degree from Dalian Maritime University, China, in 2010. She is currently with the Peng Cheng Laboratory, Shenzhen, China, and the School of Navigation, Dalian Maritime University. Since September 2012, she has been a Visiting Scholar with the Broad Band Communications Research (BBCR) Laboratory, Department of Electrical and Computer Engineering, University of Waterloo, Canada. Her research interests include edge intelligence, 6G, and maritime wideband communication networks. She serves as the Associate Editor-in-Chief for the IEEE NETWORK and *IET Communications* and an Advisory Editor for *SpringerPlus*.

Youlong Wu (Member, IEEE) received the B.S. degree in electrical engineering from Wuhan University, Wuhan, China, in 2007, the M.S. degree in electrical engineering from Shanghai Jiao Tong University, Shanghai, China, in 2011, and the Ph.D. degree from Télécom ParisTech, Paris, France, in 2014. In December 2014, he was a Post-Doctoral Researcher with the Institute for Communication Engineering, Technical University of Munich (TUM), Munich, Germany. In 2017, he joined the School of Information Science and Technology, ShanghaiTech University. He is an Alexander von Humboldt Research Fellow. He received the TUM Fellowship in 2014. His research interests include communication theory, information theory, and its applications (e.g., coded caching, distributed computation, and machine learning).

Shiyin Li received the Ph.D. degree in information and communication engineering from the China University of Mining and Technology, Xuzhou, China, in 2010. Since 2010, he has been a Professor with the School of Information and Control Engineering, China University of Mining and Technology, where he is the Head of the Department of Information Engineering. His research interests include wireless communication and network congestion control.

Naofal Al-Dhahir (Fellow, IEEE) received the Ph.D. degree from Stanford University. He is an Erik Jonsson Distinguished Professor and the ECE Associate Head with UT-Dallas. He was a Principal Member of the Technical Staff, GE Research Center; and the AT&T Shannon Laboratory, from 1994 to 2003. He is a co-inventor of 43 issued patents, the coauthor of about 500 papers, and a co-recipient of five IEEE best paper awards. He is a fellow of the National Academy of Inventors. He received the 2019 IEEE SPCC Technical Recognition Award and the 2021 Qualcomm Faculty Award. He served as the Editor-in-Chief for IEEE TRANSACTIONS ON COMMUNICATIONS, from January 2016 to December 2019.